Osmotically driven pipe flows and their relation to sugar transport in plants

KÅRE H. JENSEN[1,2], EMMANUELLE RIO [1,3] , RASMUS HANSEN[1], CHRISTOPHE CLANET[4] AND TOMAS BOHR[1]

[1]Center for Fluid Dynamics, Department of Physics,
Technical University of Denmark, Building 309, 2800 Kgs. Lyngby, Denmark

[2]Center for Fluid Dynamics, Department of Micro- and Nanotechnology,
Technical University of Denmark, DTU Nanotech Building 345 East, 2800 Kgs. Lyngby, Denmark

[3] Present address: Laboratoire de Physique des Solides, Univ. Paris-Sud, CNRS, UMR 8502, F-91405 Orsay Cedex, France.

[4]IRPHE, Universits d'Aix-Marseille, 49 Rue Frédéric Joliot-Curie
BP 146, F-13384 Marseille cedex 13, France

(Received 22 October 2008)

In plants, osmotically driven flows are believed to be responsible for translocation of sugar in the pipe-like phloem cell network, spanning the entire length of the plant. In this paper, we present an experimental and theoretical study of transient osmotically driven flows through pipes with semipermeable walls. We extend the experimental work of Eschrich, Evert and Young (Eschrich *et al.* 1972) by providing a more accurate version of their experiment allowing for better comparison with theory. In the experiments we measure the dynamics and structure of a "sugar front", i.e. the transport and decay of a sudden loading of sugar in a pipe which is closed in both ends. We include measurements of pressure inside the membrane tube allowing us to compare the experiments directly with theory and, in particular, to confirm quantitatively the exponential decay of the front in a closed tube. In a novel setup we are able to measure the entire concentration profile as the sugar front moves. In contrast to previous studies we find very good agreement between experiment and theory.

In the limit of low axial resistance (valid in our experiments as well as in many cases in plants) we show that the equations can be solved exactly by the method of characteristics yielding, in general, an implicit solution. Further we show that under more general conditions the equations of motion can be rewritten as a single integro-differential equation, which can be readily solved numerically. The applicability of our results to plants is discussed and it is shown that it is probable that the pressure-flow hypothesis can account for short distance transport of sugar in plants.

1. Introduction

The translocation of sugar in plants, which takes place in the phloem sieve tubes, is not well understood on the quantitative level. The current belief, called the pressure flow hypothesis (Nobel 1999), is based on the pioneering work of Ernst Münch in the 1920'ies (see eg. Münch 1930). It states, that the motion in the phloem is purely passive, due to the osmotic pressures that build up relatively to the neighboring xylem as a response of loading and unloading of sugar in different parts of the plant, as shown

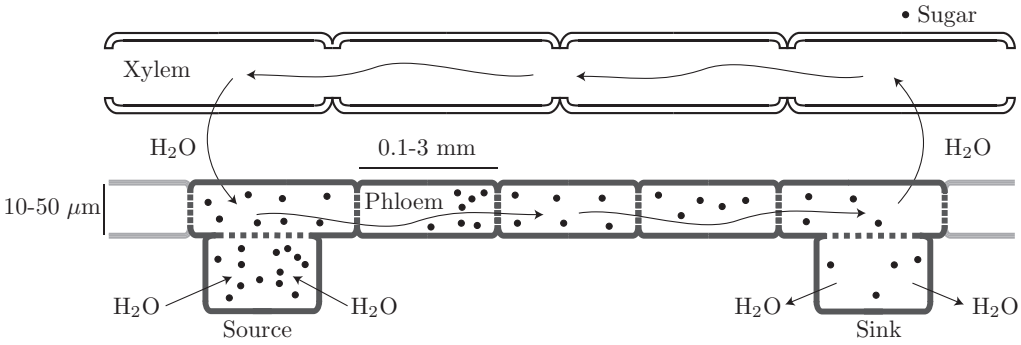

FIGURE 1. In plants, two separate pipe-like systems are responsible for the transport of water and sugar. The xylem conducts water from the roots to the shoot while the phloem conducts sugar and other nutrients from places of production to places of growth and storage. The mechanism believed to be responsible for sugar-translocation in the phloem, called the Münch mechanism or the pressure-flow hypothesis (Nobel 1999), states that following: As sugar is produced via photosynthesis in sources it is actively loaded into the tubular phloem cells. As it enters the phloem, the chemical potential of the water inside is lowered compared to the surrounding tissue, thereby creating a net flux of water into the phloem cells. This in-flux of water in turn creates a bulk flow of sugar and water towards the sugar sink shown on the right, where active unloading takes place. As the sugar is removed, the chemical potential of the water inside the phloem is raised resulting in a flow of water out of the sieve element.

in figure 1. This mechanism is much more effective than diffusion, since the osmotic pressure differences caused by different sugar concentrations in the phloem create a bulk flow directed from large concentrations to small concentrations, in accordance with the basic need of the plant. Such flows are often called Osmotically Driven Pressure Flows (Thompson & Holbrook 2003*a*), or Osmotically Driven Volume Flows (Eschrich *et al.* 1972).

It is, however, not clear how well this mechanism is able to account for the sugar translocation in plants on the quantitative level . Since the sieve tube elements that make up the phloem are living cells, the picture can indeed be much more complicated. For a large tree it would thus seem improbable that sugar transport e.g. from leaf to root by this mechanism would be sufficiently efficient, and in this case active transport processes might play an important role. On the other hand, transport over short distances, e.g. locally in leaves or from a leaf to a nearby shoot might be more convincingly described by the pressure-flow hypothesis. In any case, we need a better understanding of such flows in order to decide, whether they compare sensibly with translocation in plants, and this is the aim of the present paper. In particular, we have chosen to concentrate on transient flows caused by a sudden loading of sugar. First of all this gives us the possibility of observing dynamical behavior which allows us to compare quantitatively with theory and second, we can observe such dynamics using simple boundary conditions (e. g. closed ends), which are easily realized in experiments.

1.1. *Previous experimental work*

To study the osmotically driven flows, Eschrich, Evert and Young (Eschrich *et al.* 1972) conducted simple model experiments. Their setup consisted of a semipermeable membrane tube submerged in a water reservoir, modeling a phloem sieve element and the surrounding water-filled tissue. At one end of the tube a solution of sugar, water and dye was introduced to mimic the sudden loading of sugar into a phloem sieve element. The motion of this "sugar front" was monitored for different configurations of the tube

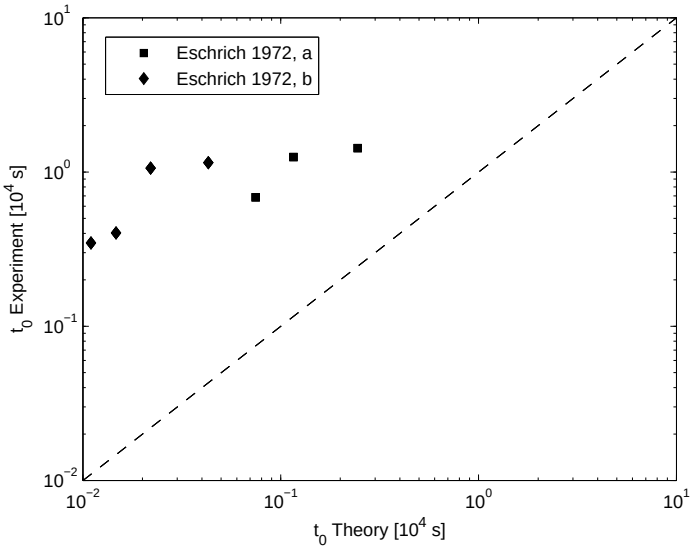

FIGURE 2. Experimental data from (Eschrich *et al.* 1972). Data points marked with an a represents results from closed tube experiments and points marked with a b represents results from semi-closed experiments. t_0^{exp} was taken from the original paper, figures 8 and 9. To calculate t_0^{theory}, the expression $t_0^{theory} = \frac{r}{2L_p\Pi}$ was used with $r = 3.5$mm and $L_p = 3.2 \times 10^{-12}\text{m(Pas)}^{-1}$. The values for Π was found from figures 8 and 9.

by observing the motion of the dyed front. They conducted experiments with the tube closed at both ends (closed) and open at one end and closed at the other (semi-closed).

In the case of the closed tube, they found that the sugar front velocity decayed exponentially as it approached the far end of the tube. Also, they found the initial velocity of the sugar front to be proportional to concentration of the sugar solution. Through simple conservation arguments, which we shall go through briefly below, they showed that for a flow driven according to the pressure-flow hypothesis, the velocity of the sugar front is given by

$$u_f = \frac{L}{t_0}\exp\left(-\frac{t}{t_0}\right) \quad \text{where} \quad t_0 = \frac{r}{2L_p\Pi}, \tag{1.1}$$

where t is time, L is the length and r is the radius of the tube, L_p is the permeability of the membrane and Π is the osmotic pressure of the sugar solution, equal to RTc (where R is the gas constant, T the absolute temperature and c the concentration in moles pr. volume) for dilute solutions of ideal molecules (Landau & Lifshitz 1980). If one applies this result to the flow inside a single sieve element ($L = 1$mm), one gets a characteristic velocity of $\simeq 7\text{mh}^{-1}$, almost an order of magnitude larger than that observed in plants (see table 3). The fact that equation 1.1 predicts a larger velocity is not surprising. One should keep in mind that the sieve cells consist of sieve elements separated by sieve plates and the resistance in strongly concentrated in the latter. Thus our experiments would model only the transport in a single sieve element without significantly changing the resistance. Secondly, the measurements in the table are supposed to be representative of a steady state situation and not the movement of a sugar front.

In their experiments Eschrich *et al.* found good qualitative agreement between their results and the prediction made by equation 1.1. However, as can be seen in figure 2, the quantitative agreement between experiments and theory was extremely poor, the theory

generally predicting decay times at least an order of magnitude smaller than observed. This discrepancy, however, is not surprising given the fact that Eschrich *et al.* did neither determine the fundamental properties of the membrane (permeability, elastic modulus), nor of the sugar (osmotic strength) independently. Also they did not take into account the unstirred concentration layers which may occur near the membrane walls, effectively lowering Π (Pedley 1980, 1981, 1983; Aldis 1988). The disagreement between theory and experiment, and the fact that the tracking of the sugar front was done indirectly, leave the details of the observed process unclear. In particular, the experiments of Eschrich *et al.* did not include a continuous monitoring of the pressure. They state (p. 295) that the turgor pressure rapidly builds up to a constant value, as predicted theoretically. They observe, however, that the tubes start leaking after around 100-150 min. (typical running time of the experiments), and this seems to indicate that the pressure continues to grow. Another source of error could come from the fact that Eschrich *et al.* used a dye for tracking the sugar front instead of directly monitoring the sugar concentration. Finally, it is not clear whether the membranes are sufficiently impermeable to the sugar (sucrose) used.

To make progress on these issues we have refined the experiments done by Eschrich *et al.* to test the pressure-flow hypothesis more accurately. We have measured the permeability of the membrane tube, and the osmotic strength of the sugar solutions independently and we continuously monitor the pressure during the experiment. Also, we have measured the elastic modulus of the membrane tube, to asses the importance of elastic effects in our system. For more detailed comparison with theory it is important to be able to assess the entire concentration profile, and to do this, we have introduced a new type of experiment, where the sugar concentration is determined directly by optical refraction.

2. Experimental setup

In our experiments, we used two setups. The first setup, from now on called setup I, is based on the design of Eschrich *et al.* , but includes continuous pressure measurements. Further, to avoid leaking of sugar across the membrane, we use a sugar (*dextran*) with a much larger molecular weight than sucrose. The second setup, Setup II, was built in the spae of a prism to be able to detect the evolution of the entire sugar profile (again using *dextran*) rather than just the front position offered by previous experiments. The two setups are discussed in detail below. Details of the sugar and semipermeable membranes can be found in appendix A.

2.1. *Setup I*

Setup I, shown on the left in figure 3, consisted of a 30 cm long, 30 mm wide glass tube in which a semipermeable membrane tube of equal length and a diameter of 10 mm was inserted. At one end, the membrane tube was fitted over a glass stopcock equipped with a rubber stoppper. At the other end, the membrane tube was fitted over a brass cylinder equipped with holder to accommodate a pressure transducer for measuring the pressure inside the membrane tube.

After filling the 30 mm wide glass tube with water, water was pressed into the semipermeable tube with the syringe. Care was taken that no air bubbles were stuck inside the tube. For introducing the sugar solution into the tube, a syringe was filled with the solution and then attached to the lower end of the stopcock which was kept closed. After fitting the syringe, the stopcock was opened and the syringe piston was very slowly pressed in, until a suitable part of the tube had been filled with the solution. Care was

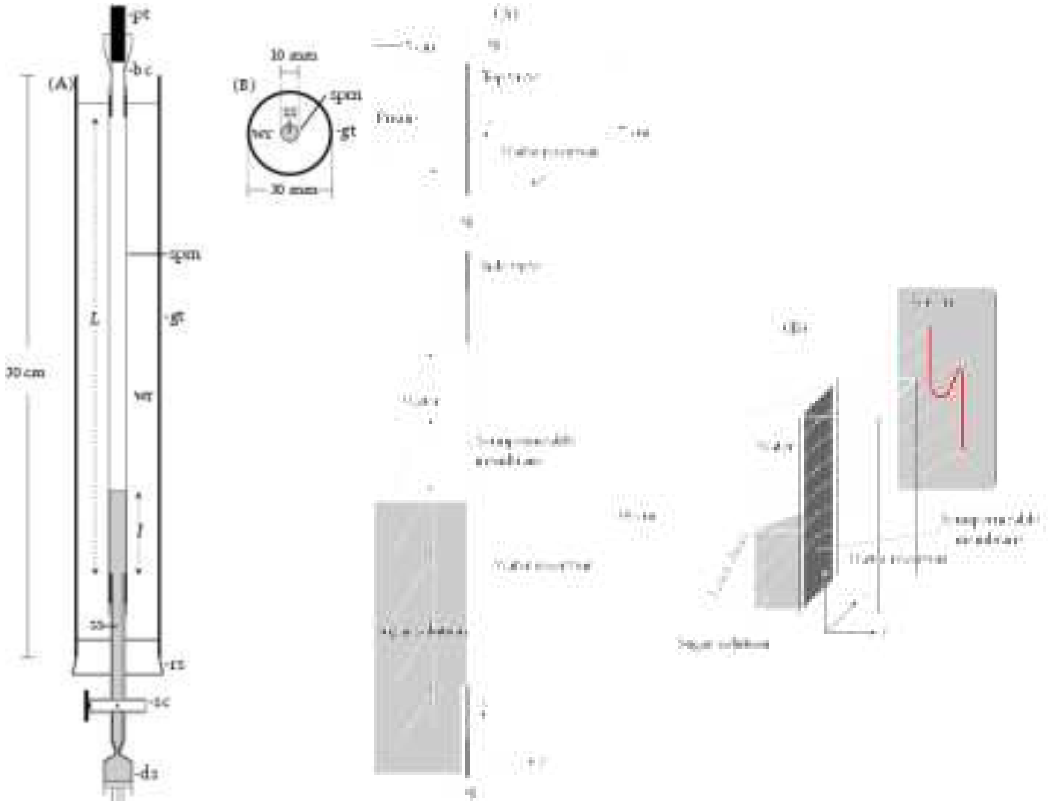

FIGURE 3. Left: Setup I used to observe the movement of a sugar-dye solution (ss) inside a semipermeable membrane tube (spm). L length of membrane tube; l initial sugar front height; ds disposable syringe; gt glass tube; rs rubber stopper; sc stopcock; wr water reservoir; bc brass cylinder; pt pressure transducer.
Right: Setup II. See details in the text.

taken to avoid any mixing between the sugar solution and the water already present in the semipermeable tube. To track the movement of the sugar solution it was mixed with a red dye and data was recorded by taking pictures of the membrane tube at intervals of 15 minutes using a digital camera. Details of how the motion of the sugar front was derived from the images is discussed in appendix B.1.

2.2. *Setup II*

Setup II, shown on the right in figure 3 consisted of a hollow isosceles glass prism and a Plexiglas cuboid in osmotic contact through a membrane. The glass prism was fitted with a pressure transducer for measuring the pressure inside the membrane tube.

When preparing an experiment, a piece of membrane was fitted in a narrow gap between the prism and the cuboid. The prism was then filled to a suitable height with a sugar solution and pure water was carefully deposited on top of the sugar solution to create a sharp sugar front. Then, the cuboid was filled with water, and the pressure transducer was mounted, thereby closing the prism.

To track the time evolution of the the sugar front inside the prism, we used the refraction of a laser sheet passing through it. The laser sheet was generated by shining a laser beam, generated by a Melles Griot 3.1 mW laser, through a glass rod. When passing through the prism, light would deviate depending on the local index of refraction.

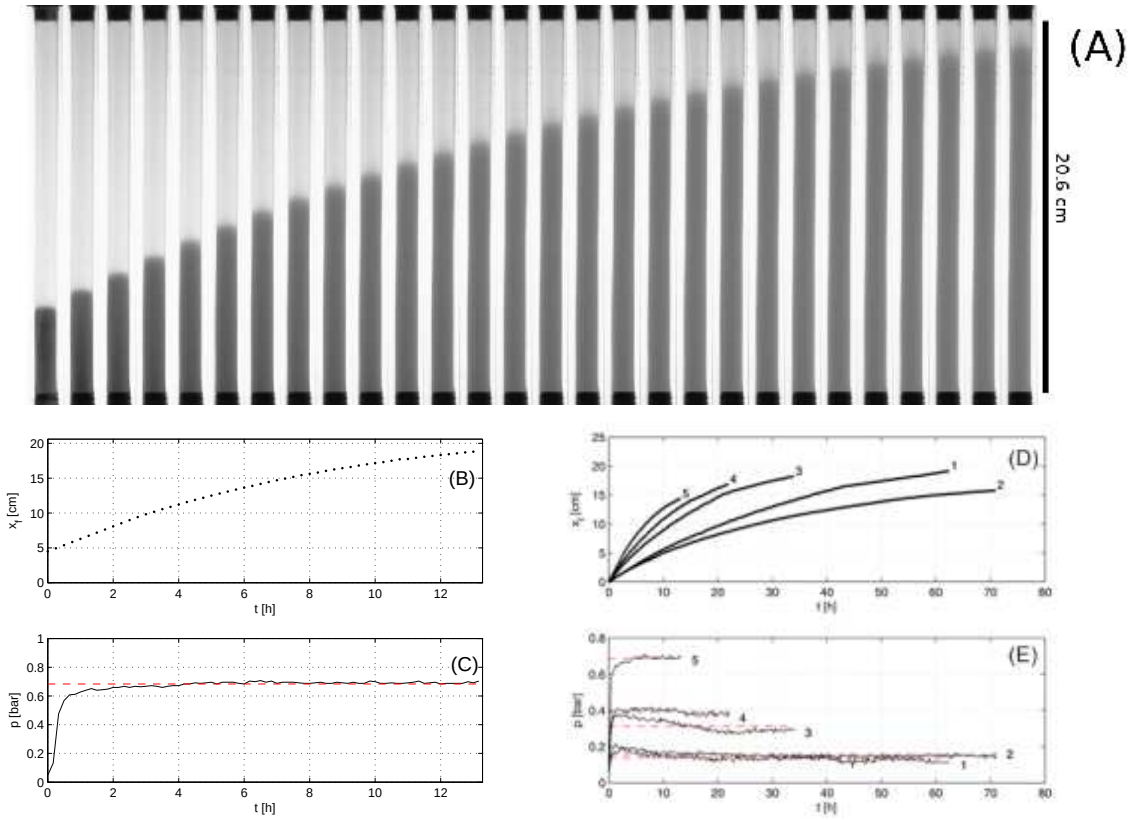

FIGURE 4. Experimental results from setup I. Top: Time series of pictures taken in experiment 5. Time increases from left to right in steps of 30 minutes. See details of the sugar solutions used in table 1. Middle, left: Plot of the front position versus time obtained from the images above. Bottom, left: Plot of the pressure inside the tube versus time. The (red) dashed line is the osmotic pressure of the solution, taken to be the average value of the pressure from $t = 2$ h until the end of the experiment. Middle, right: Plots of the sugar front position versus time for different sugar concentrations, as indicated in table 1 Bottom, right: Plots of the pressure inside the membrane tube for different sugar concentrations.

The index of refraction varies linearly with sugar concentration and thus by looking at the refracted laser sheet projected onto a screen, we were able to reconstruct the concentration profile inside the prism. A camera recorded images of the screen at regular intervals to track the moving concentration profile. The procedure used for obtaining the concentration profile inside the prism from the images aquired is discussed in appendix B.2

3. Experimental results

3.1. *Experimental results, Setup I*

The motion of the sugar front was investigated for solutions of varying sugar concentration. An example of a set of data is shown in figure 4. In (A) are the raw images, which after processing gives (B) showing the position of the sugar front, x_f, as a function of time. The errorbars on x_f are estimated to be ± 1 mm, but are too small to be seen. Finally, (C) shows the pressure inside the tube as a function of time. At first, a linear

	1	2	3	4	5
Mean sugar concentration, $\bar{c}$ [mM]	1.5±0.3	2.10±0.03	2.4±0.2	4.2±0.7	6.8±0.1
Osmotic pressure, Π [bar]	0.14 ± 0.02	0.15±0.01	0.31±0.03	0.39±0.01	0.68±0.02
Membrane tube length, L [cm]	28.5	20.8	28.5	28.5	20.6
Initial front height, l [cm]	4.9	3.7	6.6	6.5	4.8

TABLE 1. Data for the experimental runs shown in figure 4.

motion of the front is observed with a front velocity of ~ 1 cm/h. This is then followed by a decrease in the front velocity as the front approaches the end of the tube. The pressure is seen to rise rapidly during the first hour before settling to a constant value, indicated by a red, dashed line. This constant value is taken to be the osmotic pressure, Π, of the sugar solution. Looking at (A), one observes that diffusion has the effect of dispersing the front slightly as time passes. Below the front, the concentration seems to be uniform throughout the cross-section of the tube, and there is no indication of large boundary layers forming near the membrane walls.

Similar experiments with different sugar concentrations were made and a plot of the results can be seen on the right in figure 4 (D) and (E). Qualitatively both the motion of the front and of the pressure follow the same pattern as shown on the left. One notices that the speed with which the fronts move are related to the mean sugar concentration inside the membrane tube, with the high concentration solutions moving faster than the low concentration ones. The reason why 2 seems to be moving slower than 1 is that experiment 2 was conducted in a slightly shorter membrane tube than 1, thereby decreasing the characteristic velocity as we shall see later.

3.2. *Experimental results, Setup II*

Figure 5 shows the data collected using setup II. At the top, a time series of pictures is depicted showing the refracted laser-light projected onto a screen, the time between each image being one day. Comparing the upper and lower parts of each picture, one generally observes a deflection to the right at the bottom, corresponding to a high sugar concentration at the bottom of the prism. In the intermediate region one sees a dip in the refracted light, corresponding to a strong concentration gradient. The dip gradually flattens while it advances upwards, representing a sugar front which advances while it broadens. This process can be seen directly on the left in the middle row, which shows the time evolution of the sugar concentration obtained from the images. Starting from a steep concentration profile, we see that the front moves forward while it flattens. On the left in the bottom row, the time evolution of the concentration gradient is depicted, clearly showing a peak which broadens while it moves forward. Finally, on the right, the position of the sugar front and the pressure inside the prism is plotted as a function of time is shown. The errorbars on x_f are ±1 mm, found as discussed below.

3.2.1. *The effects of diffusion*

To study the effects of diffusion on the dynamics of the sugar front separately, an experiment was made with setup II, in which the membrane separating the two compartments were removed. The experiment was then prepared in the usual way, and the motion of the front recorded. The results of this is shown on the right in figure 6. Starting from a steep concentration gradient, we observe that the front flattens but otherwise does not move much.

Comparing figures 4 and 5 we observe, that while the front moves $\tilde{2}$ cm due to osmosis

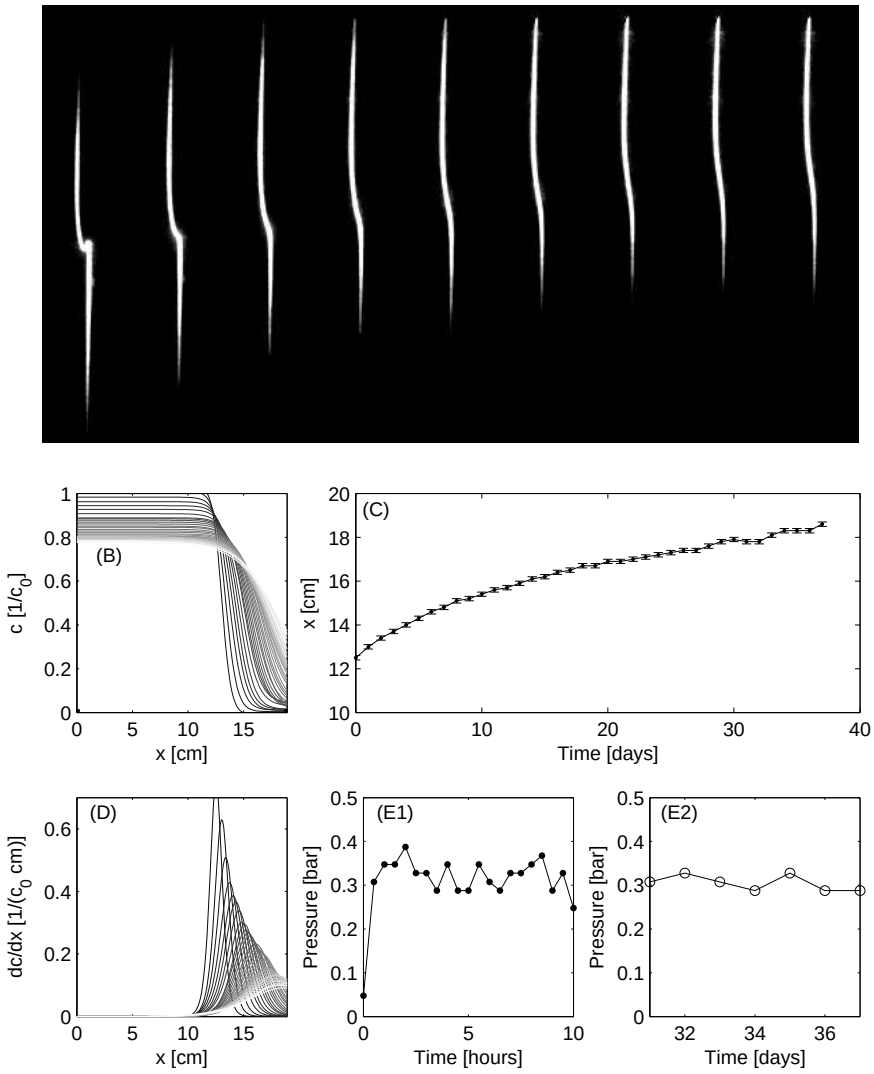

FIGURE 5. Results from setup II. In (A) the raw data images are shown. In (B) the concentration profile extracted from (A) is shown. (C) shows the front position extracted from (B) by finding the maximum of the concentration gradient, shown in (D). Finally, (E, 1-2) shows the pressure inside the prism. The dashed line indicates that the pressure sensor was accidentaly off-line. The data shows that the pressure rather quickly (within a few hours) reaches a constant level corresponding to the osmotic pressure of the sugar solution (See appendix A 2.2.)

in 72 hours, it does not move at all in 140 hours due to diffusion. Thus, while diffusion has a flattening effect, it plays little role in the forward motion of the front.

Since the front did not move due to diffusion, the fluctuations in the front position seen in figure 6 (D) gives a measure of the uncertainity of a single measurement of the front position. Taking the standard deviation of the fluctuations gives an uncertainty of ± 1 mm, shown as errorbars in figure 5 (C).

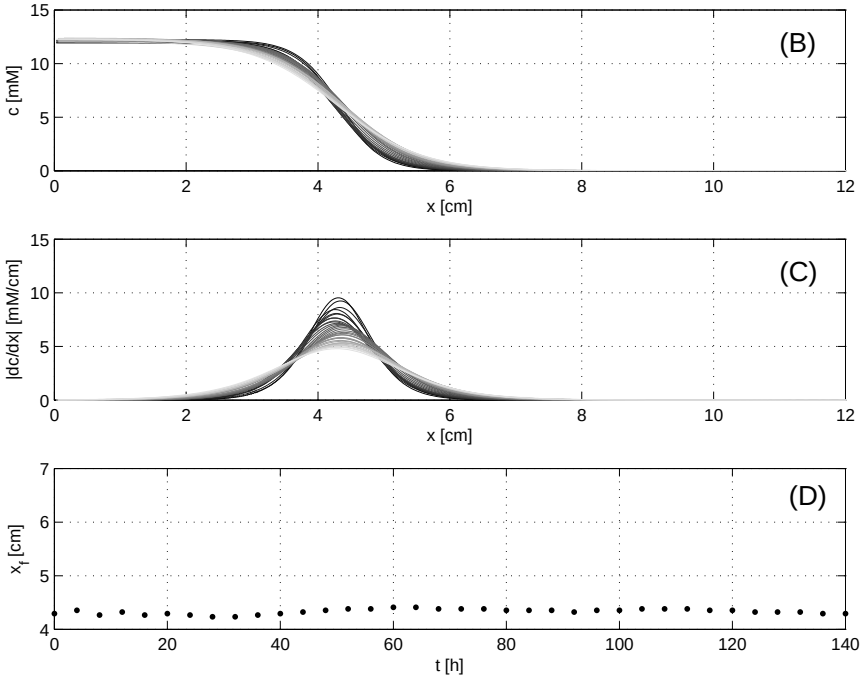

FIGURE 6. Experimental results from diffusion experiments made with setup II.

4. Theoretical analysis

4.1. *Front propagation*

Before moving on to a more thorough mathematical analysis we shall, following the analysis made by (Eschrich *et al.* 1972), show that the motion of the sugar front can be understood through simple conservation arguments. To that end, let us consider the situation in setup I. Let x_f denote the position of the sugar-dye front, and let V_1 denote the volume behind the front and V_2 that ahead of it. Taking the tube to be inelastic and the fluid inside incompressible, we must have that $\frac{dV_1}{dt} = -\frac{dV_2}{dt}$. If we let $p(x)$ and p_0 denote the hydrostatic pressure inside and outside the membrane tube and $c(x)$ the concentration averaged over the cross-section of the tube at position x, the volume flux across a unit area of the membrane is

$$J(x) = L_p \left(p_0 - p(x) + RTc(x)\right). \tag{4.1}$$

Any hydrostatic pressure gradient inside the tube will occur only due to viscous flow, but for large tubes and slow flows, this effect is entirely negligible. Thus, since

$$\int_0^L J(x')dx' = 0 \tag{4.2}$$

we get, that

$$p - p_0 = \frac{RT}{L}\int_0^L c(x')dx' \equiv RT\bar{c} \tag{4.3}$$

The rate of change of volume 2 is then

$$\frac{dV_2}{dt} = 2\pi r L_p \int_{x_f}^{L} J(x')dx' = -2\pi r L_p RT\bar{c}(L - x_f) \tag{4.4}$$

Finally, using that

$$\frac{dV_2}{dt} = -\pi r^2 \frac{dx_f}{dt} \tag{4.5}$$

we get for the front position

$$\frac{dx_f}{dt} = \frac{2L_p RT\bar{c}}{r}(L - x_f) = \frac{1}{\tau}(L - x_f) \tag{4.6}$$

which has the solution

$$x_f(t) = L - (L - l)\exp\left(-\frac{t}{\tau}\right) \tag{4.7}$$

where $l = x_f(0)$ is the position of the front at $t = 0$. This simple result, shows that the relaxation time

$$\tau = \frac{r}{2L_p RT\bar{c}} \tag{4.8}$$

for the front propagation depends only on three quantities; the membrane permeability, the osmotic pressure of the sugar solution and the ratio of membrane circumference to cross-section area.

The neglect of elastic deformations of the tube is appropriate for the experiments made in both setups, as shown in Appendix A.2, as long as the pressures remain below around 1.2 bars. Since we use the large dextran molecules, the osmotic pressures remain well below this limit. When sucrose is used, pressures become much larger and elastic properties can become important. In Appendix E, we show how the above results would change, if elastic properties are taken into account.

4.2. *Derivation of the flow equations*

To formalize the assumptions made above, we will now derive the equations of motion for osmotically driven flows, with the geometry of setup I in mind. In appendix C, we shall see that under certain conditions the equations are also valid in other geometries, such as the triangular geometry of setup II.

The equations of motion for osmotically driven flows have been derived and analyzed thoroughly several times in the literature (see eg. Weir 1981) and have been studied carefully numerically, (Thompson & Holbrook 2003*a*,*b*; Henton 2002). For the sake of completeness, we shall include a short derivation of these.

We consider a tube of length L and radius r, as shown in figure (7). The tube has a constant cross section of area $A = \pi r^2$ and circumference $S = 2\pi r$ and its walls are made of a semipermeable membrane with permeability L_p. Inside the tube is a solution of sugar and water with concentration $c(x)$. Throughout this paper, we shall study the transient dynamics generated by an asymmetrical initial concentration distribution, where the sugar is initially localised to one end of the tube with a concentration level c_0. The tube is surrounded by a water reservoir, modelling the water surrounding the membrane tube in setup I.

We shall assume that $L \gg r$ and that the radial component of the flow velocity inside the tube is much smaller than the axial component, as is indeed the case in the experiments. With these assumptions, we will model the flow in the spirit of lubrication theory and consider only a single average axial velocity component $u(x, t)$. Also, we will

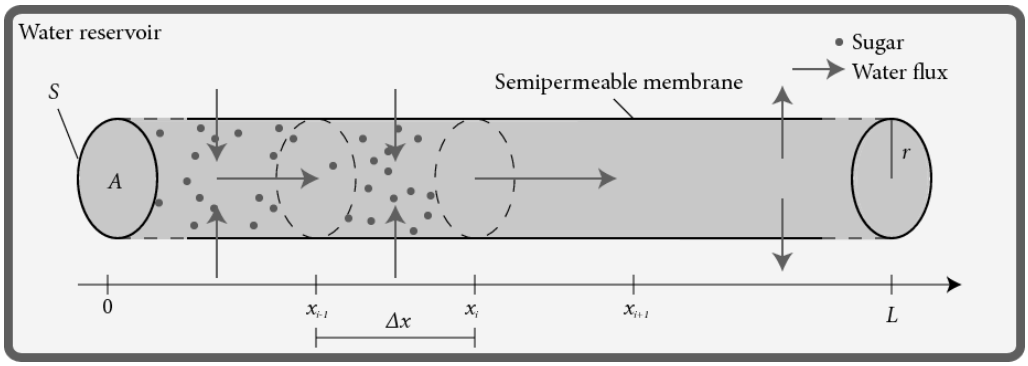

FIGURE 7. Sketch of the tube.

assume that the concentration, c, is independent of the radial position, ρ, an assumption that can be verified experimentally in setup II.

Let us now consider the equation of volume conservation by looking at a small section of tube between x_{i-1} and x_i. The volume flux into the section due to advection is

$$A(u_{i-1} - u_i), \tag{4.9}$$

where the axial flow velocities are taken to be u_{i-1} and u_i at x_{i-1} and x_i, respectively. The volume flux inwards across the membrane due to osmosis (see eg. Schultz 1980) is

$$S\Delta x L_p(RTc - p). \tag{4.10}$$

where p is the pressure. For clarity we use the van't Hoff value $\Pi = RTc$ for the osmotic pressure, which is only valid for ideal solutions. When comparing with experiments we replace this by $\Pi = \gamma c$, where γ must be experimentally determined (see appendix A.2), and thus only use that Π is linear in c for small concentrations. Assuming conservation of volume, we get that

$$A(u_{i-1} - u_i) + S\Delta x L_p(RTc - p) = 0 \tag{4.11}$$

Letting $\Delta x \to 0$ and using that the cross-section to perimeter ratio reduces to $\frac{r}{2}$, this becomes

$$\frac{r}{2}\frac{\partial u}{\partial x} = L_p(RTc - p) \tag{4.12}$$

For these very slow and slowly varying flows, the time dependence of the Navier-Stokes equation can be neglected and the velocity field is determined by the instantaneous pressure gradient though the Poiseuille or d'Arcy relation (for a circular tube)

$$u = -\frac{r^2}{8\eta}\frac{\partial p}{\partial x}, \tag{4.13}$$

where η is the dynamic viscosity of the solution, typically $\sim 1.5 \times 10^{-3}$ Pa s in our experiments.

Differentiating equation (4.12) with respect to x and inserting the result from equation (4.13) we get for the conservation of water that

$$RT\frac{\partial c}{\partial x} = \frac{r}{2L_p}\frac{\partial^2 u}{\partial x^2} - \frac{8\eta}{r^2}u. \tag{4.14}$$

The final equation expresses the conservation of sugar advected with veolcity u and

	M	$\bar{D}$
Setup I	2×10^{-8}	6×10^{-5}
Setup II	10^{-9}	2×10^{-2}
Single Sieve element ($L = 1$ mm)	5×10^{-4}	5×10^{-4}
Leaf ($L = 1$ cm)	5×10^{-2}	5×10^{-5}
Branch ($L = 1$ m)	5×10^{2}	5×10^{-7}
Small tree ($L = 10$ m)	5×10^{4}	5×10^{-8}

TABLE 2. Values of the parameters M and $\bar{D}$ in various situations.

diffusing with molecular diffusivity D

$$\frac{\partial c}{\partial t} + \frac{\partial uc}{\partial x} = D\frac{\partial^2 c}{\partial x^2}. \tag{4.15}$$

The set of equations 4.14–4.15 are equivalent to those of Thompson and Holbrook (Thompson & Holbrook 2003*b*) except for the fact that we have removed the pressure by substitution, and that we do not consider elastic deformations of the tube.

4.2.1. *Non-dimensionalization of the flow equations*

To non-dimensionalize equations (4.14) and (4.15), we introduce the following scaling

$$c = c_0 C, \qquad u = u_0 U, \qquad x = LX, \qquad t = t_0 \tau.$$

L has been chosen such that the spatial domain is now the unit interval $X \in [0, 1]$, $u_0 = L/t_0$ and c_0 is the initial concentration level in one end of the tube. Choosing further

$$t_0 = \frac{r}{2L_p RTc_0}, \quad M = \frac{16\eta L^2 L_p}{r^3} \quad \text{and} \quad \bar{D} = \frac{D}{u_0 L} = \frac{Dr}{2RTc_0 L^2 L_p}, \tag{4.16}$$

and inserting in equations 4.14 and 4.15, we get the non-dimensional flow equations.

$$\frac{\partial^2 U}{\partial X^2} - MU = \frac{\partial C}{\partial X}, \tag{4.17}$$

$$\frac{\partial C}{\partial \tau} + \frac{\partial UC}{\partial X} = \bar{D}\frac{\partial^2 C}{\partial X^2}. \tag{4.18}$$

Going back to the original notation

$$X \to x, \qquad U \to u, \qquad C \to c, \qquad \tau \to t$$

we finally obtain

$$\frac{\partial^2 u}{\partial x^2} - Mu = \frac{\partial c}{\partial x}, \tag{4.19}$$

$$\frac{\partial c}{\partial t} + \frac{\partial uc}{\partial x} = \bar{D}\frac{\partial^2 c}{\partial x^2}. \tag{4.20}$$

The parameter M corresponds to the ratio of axial to membrane flow resistance, which we shall refer to as the *Münch number*. This is identical to the parameter $\hat{F}$ in Thompson & Holbrook (2003*b*). The second parameter $\bar{D}$ is the ratio of diffusive and advective solute flux. Thus, the longer the tube is the less important diffusion becomes and the more important the pressure gradient due to viscous effects become.

Values of the parameters M and $\bar{D}$ in different situations can be seen in table 2. The

Quantity	Magnitude	Reference.
Radius [μm]	4.5 (Fava bean), 4 (Winter squash), 6–25	†, ∗, ||
Length [mm]	0.09 (Fava bean), 0.1–3	†, ||
Flow velocity [mh^{-1}]	0.5–1, 0.2–2	†, ||
Elastic Modulus [MPa]	17, 5.6–7.4 (Ash)	•, ⟨
Permeability [10^{-11} ms^{-1}Pa^{-1}]	5,1.1 (Zitella translucence)	•, ⟩
Sucrose concentration [M]	0.3–0.9	∗

TABLE 3. Characteristic properties of phloem sieve elements. References: † Knoblauch & van Bel (1998), ∗ Taiz & Zeiger (2002), || Nobel (1999), • Thompson & Holbrook (2003*a*), ⟨ Niklas (1992), ⟩ Eschrich *et al.* (1972).

typical magnitude of the parameters M and $\bar{D}$ in plants are found from the values also given in table 2:

$$r = 10\ \mu\text{m}, \qquad \eta = 1.5 \times 10^{-3}\ \text{Pas}, \qquad u_0 = 2\ \text{mh}^{-1}, \qquad L_p = 2 \times 10^{-11}\text{m(Pas)}^{-1}.$$

We observe, that M and $\bar{D}$ are small in both experiments, and that for short distance transport in plants this is also the case. However, over length-scales comparable to a branch ($L = 1$ m) or a small tree ($L = 10$ m) M is large, so in this case the pressure gradient is not negligible.

When deriving the equations for osmotically driven flows, we have assumed that the concentration inside the tube was a function of x and t only. However, the real concentration inside the tube will also depend on the radial position ρ in the form of a concentration boundary layer near the membrane, in the literature called an *unstirred layer* (Pedley 1983) Close to the membrane, the concentration c_m is lowered compared to the bulk value, c_b, because sugar is advected away from the membrane by the influx of water. This, in turn, results in a lower influx of water, ultimately causing the axial flow inside the tube to be slower than expected. In our experiments we see no signs of such boundary layers and apparently their width and the effects on the bulk flow are very small.

5. Solution of the flow-equations

The equations governing the time evolution of a sharp sugar front has been known for the closed and semi-closed tube since the work of Eschrich *et al.* . However, their solutions yield only the position of the front, and not the concentration profiles in front of and behind the concentration front. Analytic solutions giving the time evolution of the entire concentration profile has been found for the closed tube for $M = \bar{D} = 0$ by G. J. Weir (Weir 1981) and by H. L. Frisch (Frisch 1976) for the the semi-closed tube for $M = 0$, $\bar{D} \neq 0$. In both cases the authors have started from piecewise constant Heaviside-like initial concentration profile. To extend this work, we shall present a method for solving the equations of motions analytically using Riemann's method of characteristics. For an arbitrary initial condition, this method will generally yield an implicit solution. Only in special cases will it yield a closed formula for the solution. The method works for $M = \bar{D} = 0$ and for closed and semi-closed tube geometries.

For arbitrary values of M and $\bar{D}$, we cannot solve the equations of motion analytically and thus have to use numerical methods. This topic has been the focus of much work both in the steady-state case (Thompson & Holbrook 2003*a*) and in the transient case (Henton 2002). However, no formulation capable of handling all different boundary conditions has so far been presented. Therefore, we show that using Green's functions, the equations

of motion can be transformed into a single integro-differential equation, which can be solved using standard numerical methods.

5.1. *Results for small Münch number*

In the limit $M = \bar{D} = 0$ the equations become

$$\frac{\partial^2 u}{\partial x^2} = \frac{\partial c}{\partial x}, \tag{5.1}$$

$$\frac{\partial c}{\partial t} + \frac{\partial uc}{\partial x} = 0. \tag{5.2}$$

By integrating equation equation 5.1 with respect to x, we get that

$$\frac{\partial u}{\partial x} = c + F(t). \tag{5.3}$$

If we choose $u(0) = u(1) = 0$, $F(t)$ becomes

$$F(t) = -\int_0^1 c\, dx \equiv -\bar{c}(t), \tag{5.4}$$

Using 5.3 in equation 5.2 gives

$$\frac{\partial}{\partial x}\left(\frac{\partial u}{\partial t} + u\left(\frac{\partial u}{\partial x} + \bar{c}\right)\right) = 0. \tag{5.5}$$

Integrating with respect to x and using the boundary conditions on u, this becomes

$$\frac{\partial u}{\partial t} + u\frac{\partial u}{\partial x} = -\bar{c}u. \tag{5.6}$$

Equation 5.6 is a damped Burgers equation (see eg. Gurbatov *et al.* 1991), which can be solved using Riemann's method of characteristics. The characteristic equations are

$$\frac{\mathrm{d}u}{\mathrm{d}t} = -\bar{c}u \tag{5.7}$$

$$\frac{\mathrm{d}x}{\mathrm{d}t} = u. \tag{5.8}$$

Equation 5.7 has the solution

$$u = u_0(\xi)\exp(-\bar{c}t), \tag{5.9}$$

where the parametrization $\xi(x,t)$ of the initial velocity has to be found from

$$x = \xi + \frac{1}{\bar{c}}u_0(\xi)\left(1 - \exp(-\bar{c}t)\right) \tag{5.10}$$

where $\xi = x$ at $t = 0$.

5.1.1. *Solution for piecewise constant initial concentration*

To be able compare our method to the results obtained by (Weir 1981), we will use a Heaviside step function as initial condition on c

$$c(x, t=0) = c_I H(\lambda - x) = \begin{cases} c_I & \text{for} \quad 0 \le x \le \lambda, \\ 0 & \text{for} \quad \lambda < x \le 1, \end{cases} \tag{5.11}$$

Equation 5.3 now enables us to find the initial condition on the velocity

$$u(x,t=0) = \int_0^x (c(x',0) - \bar{c})\, dx' = \int_0^x (c(x',0) - \lambda c_I)\, dx' \tag{5.12}$$

$$= \begin{cases} (c_I - \bar{c})x & \text{for} \quad 0 \le x \le \lambda, \\ \bar{c}(1-x) & \text{for} \quad \lambda < x \le 1, \end{cases} \tag{5.13}$$

From equation 5.13, we have that

$$u_0(\xi) = \begin{cases} (c_I - \bar{c})\xi & \text{for} \quad 0 \le \xi \le \lambda, \\ \bar{c}(1-\xi) & \text{for} \quad \lambda < \xi \le 1. \end{cases} \tag{5.14}$$

Then, solving for $\xi(x,t)$ in equation 5.10 gives

$$\xi(x,t) = \begin{cases} \frac{x}{1+\frac{1}{\lambda}(1-\lambda)(1-\exp(-\bar{c}t)} & \text{for} \quad x \in I_1 \\ \frac{x-1+\exp(-\bar{c}t)}{\exp(-\bar{c}t)} & \text{for} \quad x \in I_2 \end{cases} \tag{5.15}$$

where the intervals I_1 and I_2 are defined by

$$I_1 = [0, 1 - (1-\lambda)\exp(-\bar{c}t)], \tag{5.16}$$

$$I_2 = [1 - (1-\lambda)\exp(-\bar{c}t), 1]. \tag{5.17}$$

Finally, $u(x,t)$ is calculated from equation 5.9

$$u(x,t) = \begin{cases} \frac{(c_I - \bar{c})\exp(-\bar{c}t)x}{\frac{1}{\lambda}(1-\lambda)(1-\exp(-\bar{c}t))}, & \text{for} \quad x \in I_1 \\ \bar{c}(1-x), & \text{for} \quad x \in I_2 \end{cases} \tag{5.18}$$

which is equivalent to the result obtained by (Weir 1981). The solution is plotted in figure 8, top. We can now calculate the instantaneous sugar front position x_f and velocity u_f using the right boundary of I_1 from equation 5.16

$$x_f(t) = 1 - (1-\lambda)\exp(-\bar{c}t), \tag{5.19}$$

$$u_f(t) = \frac{\mathrm{d}x_f}{\mathrm{d}t} = \bar{c}(1-\lambda)\exp(-\bar{c}t). \tag{5.20}$$

Similarly, $c(x,t)$ is given by

$$c(x,t) = \frac{\bar{c}}{1-(1-\lambda)\exp(-\bar{c}t)} H(x_f - x). \tag{5.21}$$

Going back to dimensional variables, equations (5.19) and (5.20) become

$$x_f(t) = L - (L-l)\exp\left(-\frac{t}{\tau}\right) \quad \text{and} \tag{5.22}$$

$$u_f(t) = \frac{L}{\tau}\exp\left(-\frac{t}{\tau}\right), \tag{5.23}$$

where L is the length of the membrane tube, l is the initial front position and the decay-time τ is accordance with the simple argument leading to equation (4.8).

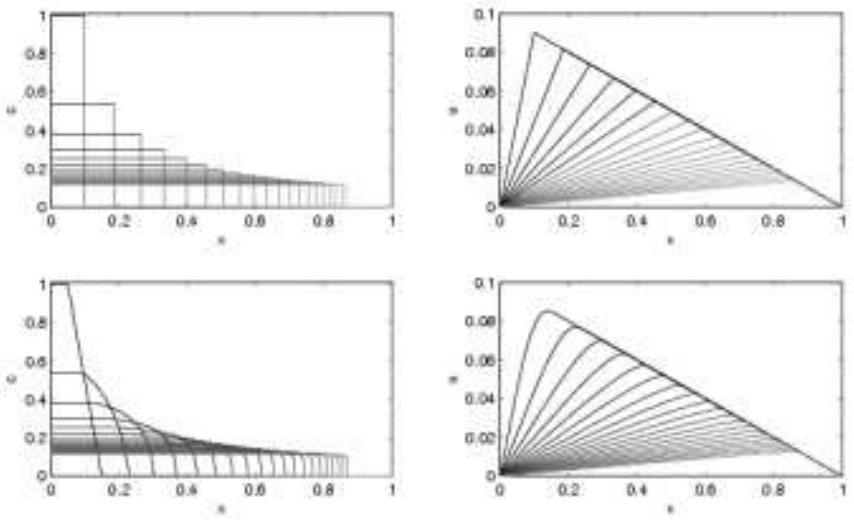

f

FIGURE 8. Top: Plot of the analytical solution for a piecewise constant initial concentration. $\lambda = 0.1$, $c_I = 1$ and $\bar{c} = 0.1$. Bottom: Plot of the analytical solution for a piecewise linear initial concentration. $\lambda_1 = 0.05$, $\lambda_2 = 0.15$, $c_I = 1$ and $\bar{c} = 0.1$. Time increases from black to gray in steps of one unit of time.

5.1.2. *Solution for piecewise linear initial concentration*

As initial condition on c, we will use the piecewise linear concentration profile given by

$$c(x, t=0) = \begin{cases} c_I & \text{for} \quad 0 \le x \le \lambda_1, \\ c_I \frac{\lambda_2 - x}{\lambda_2 - \lambda_1} & \text{for} \quad \lambda_1 \le x \le \lambda_2, \\ 0 & \text{for} \quad \lambda_2 < x \le 1, \end{cases} \tag{5.24}$$

Using 5.3 yields the initial velocity

$$u(x, t=0) = \begin{cases} (c_I - \bar{c})x & \text{for} \quad 0 \le x \le \lambda_1, \\ A_1 x^2 + B_1 x + C_1 & \text{for} \quad \lambda_1 \le x \le \lambda_2, \\ \bar{c}(1-x) & \text{for} \quad \lambda_2 < x \le 1, \end{cases} \tag{5.25}$$

where $\bar{c} = c_I \frac{\lambda_1 + \lambda_2}{2}$, and the constants are given by

$$A_1 = -\frac{c_I}{2(\lambda_2 - \lambda_1)}, \qquad B_1 = \frac{c_I \lambda_2}{\lambda_2 - \lambda_1} - \bar{c}, \qquad C_1 = c_I \lambda_1 + \frac{c_I}{\lambda_2 - \lambda_1} \left(\lambda_1 \lambda_2 + \lambda_1^2 / 2 \right). \tag{5.26}$$

Finding $\xi(x, t)$ from equation 5.10 now gives, that

$$\xi(x,t) = \begin{cases} \frac{x}{1 + \frac{1}{\lambda}(1-\lambda)(1 - \exp(-\bar{c}t)} & \text{for} \quad x \in I_1, \\ A_2 \xi_2^2 + B_2 \xi_2^2 + C_2 & \text{for} \quad x \in I_2, \\ \frac{x - 1 + \exp(-\bar{c}t)}{\exp(-\bar{c}t)} & \text{for} \quad x \in I_3, \end{cases} \tag{5.27}$$

where

$$A_2 = \frac{A_1}{\bar{c}}(1-\exp(-\bar{c}t)), \qquad B_2 = 1+\frac{B_1}{\bar{c}}(1-\exp(-\bar{c}t)), \qquad C_2 = \frac{C_1}{\bar{c}}(1-\exp(-\bar{c}t)), \tag{5.28}$$

and

$$\xi_2 = \frac{-B_2+\sqrt{B_2^2-4A_2(C_2-x)}}{2A_2}, \tag{5.29}$$

where the plus solution has been chosen to ensure, that $\xi \to x$ as $t \to 0$. Finally,

$$I_1 = \left[0, \lambda_1 + \frac{\lambda_1}{\bar{c}}(c_I-\bar{c})(1-\exp(-\bar{c}t))\right], \tag{5.30}$$

$$I_2 = \left[\lambda_1 + \frac{\lambda_1}{\bar{c}}(c_I-\bar{c})(1-\exp(-\bar{c}t)), 1-(\lambda_2-1)\exp(-\bar{c}t)\right], \tag{5.31}$$

$$I_3 = \left[1-(\lambda_2-1)\exp\left(-\bar{c}t\right), 1\right]. \tag{5.32}$$

Plugging into 5.9 gives $u(x,t)$ as

$$u(x,t) = \begin{cases} \frac{(c_I-\bar{c})\exp(-\bar{c})x}{1+\frac{1}{\lambda}(1-\lambda)(1-\exp(-\bar{c}t)} & \text{for} \quad x \in I_1, \\ \left(A_1\xi_2^2 + B_1\xi_2^2 + C_1\right)\exp(-\bar{c}t) & \text{for} \quad x \in I_2, \\ \bar{c}\,(1-x) & \text{for} \quad x \in I_3, \end{cases} \tag{5.33}$$

as shown in figure 8 along with c found from equation 5.3.

5.2. *Results for large Münch number*

In the limit of large $M \gg 1$ we cannot neglect the pressure gradient along the channel and this term dominates the advective term in (4.14), i.e. the second derivative in u. Thus

$$\frac{\partial c}{\partial x} = -Mu \tag{5.34}$$

$$\frac{\partial c}{\partial t} + \frac{\partial cu}{\partial x} = \bar{D}\frac{\partial^2 c}{\partial x^2} \tag{5.35}$$

giving the nonlinear diffusion equation

$$\frac{\partial c}{\partial t} = M\frac{\partial}{\partial x}\left[c\frac{\partial c}{\partial x}\right] + D\frac{\partial^2 c}{\partial x^2} \tag{5.36}$$

If we neglect molecular diffusion, which is true as long as $Mc \gg \bar{D} \approx 10^{-5}$, the resulting universal nonlinear diffusion equation can be written

$$\frac{\partial c}{\partial t} = M\frac{\partial}{\partial x}\left[c\frac{\partial c}{\partial x}\right] \tag{5.37}$$

which belongs to a class of equations which have been studied e.g. in the context of intense thermal waves by Zeldovich et al. and flow through porous media by Barenblatt (Barenblatt 1996) in the 50'ies. The Münch number M can be removed by rescaling the time according to $T = Mt$, so in this limit we get very slow motion with a time scale growing linearly with M. The equation (5.37) admits scaling solutions of the form

$$c(x,t) = (Mt)^\alpha \Phi(\xi) \quad \text{with} \quad \xi = x(Mt)^\beta \tag{5.38}$$

as long as $\alpha + 2\beta + 1 = 0$. The total amount of sugar is, however, conserved. In our rescaled units

$$\int_0^1 c(x)\,\mathrm{d}x = \lambda \tag{5.39}$$

where, as before, λ is the fraction of the tube initially containing the sugar. We can only hope to find a scaling solution in the intermediate time-regime, where the precise initial condition has been forgotten, but the far end ($x = 1$) is not yet felt. Thus we can replace the integral (5.39) with

$$\int_0^\infty c\,\mathrm{d}x = \lambda \tag{5.40}$$

which implies that $\alpha = \beta = -1/3$ and

$$c(x,t) = (Mt)^{-1/3}\Phi(\xi) \quad \text{with} \quad \xi = \frac{x}{(Mt)^{1/3}} \tag{5.41}$$

Inserting this form into (5.37), we obtain the differential equation for Φ

$$\frac{1}{2}\frac{d^2\Phi^2}{d\xi^2} + \frac{1}{3}\frac{d(\xi\Phi)}{d\xi} = 0 \tag{5.42}$$

which can be integrated once to

$$\Phi\frac{d\Phi}{d\xi} + \frac{1}{3}\xi\Phi = \text{const} \tag{5.43}$$

Due to the boundary condition $\partial c/\partial x = 0$ in the origin, the constant has to vanish and we find the solution

$$\Phi(\xi) = \frac{1}{6}(b^2 - \xi^2) \tag{5.44}$$

which is valid only for ξ less that the constant b. For $\xi > b$, Φ is identically 0. The fact that the solution - in contrast to the linear diffusion equation - has *compact support*, is an interesting characteristic of a large class of nonlinear diffusion equations (Barenblatt 1996). The value of b is determined by the conservation integral (5.40) giving $\int_0^\infty \Phi\,\mathrm{d}\xi = 1$, and thus $b = (9\lambda)^{1/3}$.

The final solution thus has the form

$$c(x,t) = \begin{cases} \frac{1}{6Mt}\left((x_f(t))^2 - x^2\right) & \text{for} \quad x < x_f(t) = (9\lambda Mt)^{1/3} \\ 0 & \text{for} \quad x > x_f(t) \end{cases} \tag{5.45}$$

which shows that the sugar front moves as $x_f(t) \sim t^{1/3}$ and the concentration at the origin decays as $c(0,t) \sim t^{-1/3}$. To check the validity of this solution, also when the initial condition has support in a finite region near the origin, we plot $(\bar{c}L)^{-2/3}(Mt)^{1/3}c(x,t)$ against $\xi = x(\bar{c}LMt)^{-1/3}$ in figure 9, C.

5.3. *Numerical methods for nonzero M and $\bar{D}$*

For nonzero values of M and $\bar{D}$, the equations of motion,

$$\frac{\partial^2 u}{\partial x^2} - Mu = \frac{\partial c}{\partial x} \tag{5.46}$$

and

$$\frac{\partial c}{\partial t} + \frac{\partial cu}{\partial x} = \bar{D}\frac{\partial^2 c}{\partial x^2} \tag{5.47}$$

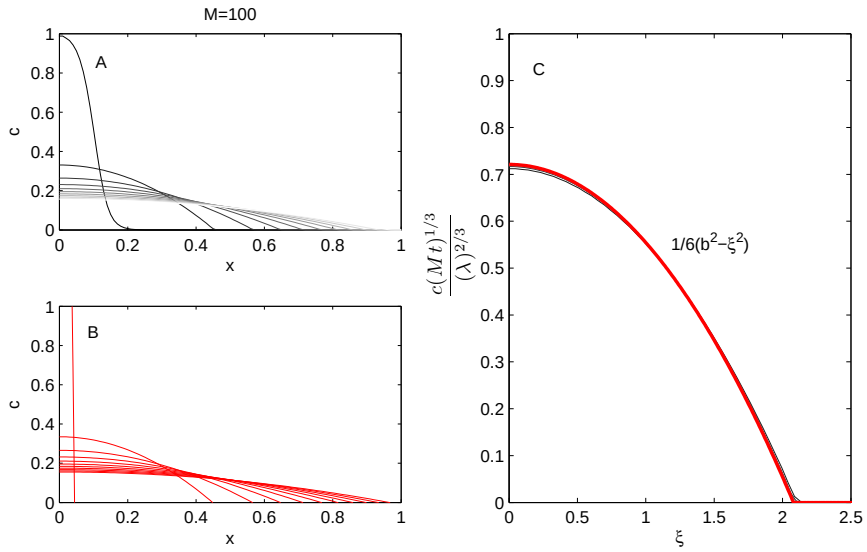

FIGURE 9. (A) Numerical simulation of equation (5.37) compared with (B) the scaling solution (5.45) and (C) (5.44). The intial condition has the form $c(x,0) = 1 - \frac{1}{1+\exp\left(-\frac{x-\lambda}{\epsilon}\right)}$ where $\lambda = 0.1$ and $\epsilon = 2 \times 10^{-2}$ and the curves are equidistant in time. When λ controlling the size of the region of nonzero initial sugar concentration becomes larger, a more accurate scaling solution is found by letting $t \to t + t_0$ and treating t_0 as an unknown parameter. In (C), we have omitted the first curve (the initial condition).

cannot be solved analytically. However, they can be written as a single integro-differential equation, which is straightforward to solve on a computer. If we choose a set of linear boundary conditions, $B_x[u] = a_i$, for equation 5.46, the solution can be written as

$$u = \int_0^1 G(x,\xi)\frac{\partial c}{\partial \xi}d\xi + u_2. \tag{5.48}$$

Here, $G(x,\xi)$ is the Green's function for the differential operator $\frac{\partial^2}{\partial x^2} - M$ with boundary conditions $B_x[u] = 0$ and u_2 fulfills the homogeneous version of 5.46 with $B_x[u] = a_i$. Plugging this into equation 5.47 yields

$$\frac{\partial c}{\partial t} + \frac{\partial}{\partial x}\left(c\left(\int_0^1 G(x,\xi)\frac{\partial c}{\partial \xi}d\xi + u_2\right)\right) = \bar{D}\frac{\partial^2 c}{\partial x^2} \tag{5.49}$$

For the closed tube, ie. for the boundary conditions $u(0,t) = u(1,t) = 0$, $G(x,\xi)$ is given by

$$G(x,\xi) = \begin{cases} -\frac{\sinh(a(1-x))}{a\sinh a}\sinh a\xi & \text{for} \quad \xi < x, \\ -\frac{\sinh ax}{a\sinh a}\sinh(a(1-\xi)) & \text{for} \quad \xi > x, \end{cases} \tag{5.50}$$

and $u_2 = 0$. To increase numerical accuracy, it is convenient to transform equation 5.49 by defining

$$\frac{\partial f}{\partial x} = c - \bar{c} \tag{5.51}$$

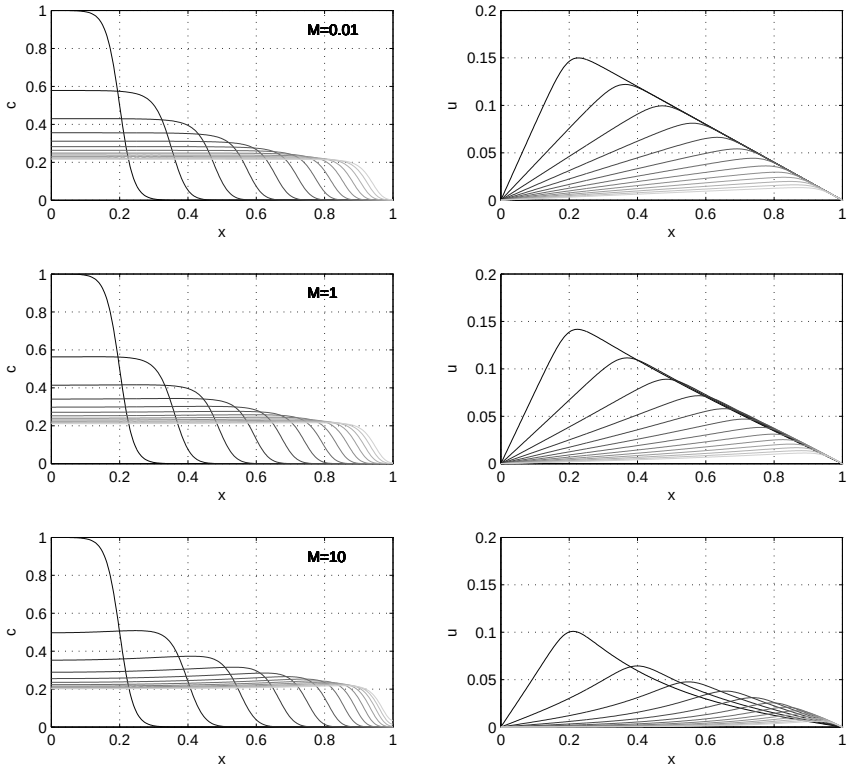

FIGURE 10. Results of numerical simulation of equation 5.49 using the boundary conditions $u(0,t) = u(1,t) = 0$ for different values of M. $\bar{D}$ is kept constant at 10^{-5}. The initial condition was $c(x,0) = 1 - \frac{1}{1+\exp\left(-\frac{x-\lambda}{\epsilon}\right)}$ where $\lambda = 0.2$ and $\epsilon = 2 \times 10^2$

and choosing $f(0) = f(1) = 0$ such that $f(x) = \int_0^x (c - \bar{c})\, d\xi$. Inserting in equation 5.49, we get that

$$\frac{\partial f}{\partial t} = \bar{D}\frac{\partial^2 f}{\partial x^2} - \left(f(x) - \int_0^1 \frac{\partial K(x,\xi)}{\partial \xi} f(\xi)\, d\xi \right) \left(\frac{\partial f}{\partial x} + \bar{c} \right), \tag{5.52}$$

where

$$\frac{\partial K(x,\xi)}{\partial \xi} = \begin{cases} -a\frac{\sinh(a(1-x))}{\sinh a}\sinh a\xi & \text{for} \quad \xi < x, \\ -a\frac{\sinh ax}{\sinh a}\sinh(a(1-\xi)) & \text{for} \quad \xi > x. \end{cases} \tag{5.53}$$

To solve equation 5.52 we used MATLAB's built-in time solver `ode23t` which is based on an explicit Runge-Kutta formula along with standard second order schemes for the first and second order derivatives. For the spatial integration, the trapezoidal rule was used (Press 2001). The numerical code can be found in appendix D. Results of a numerical simulation for different values of M is shown in figure 5.3

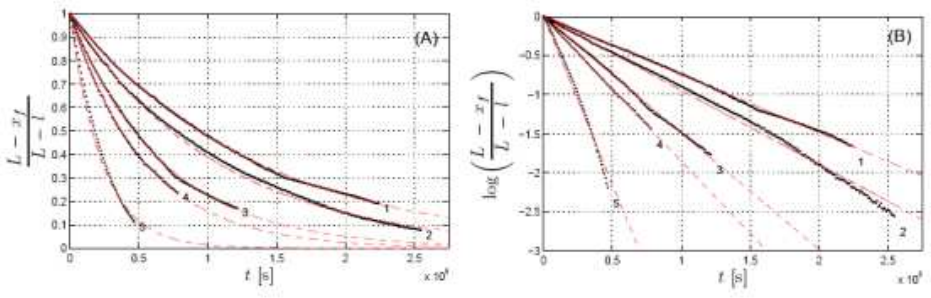

FIGURE 11. (A): Experimental (black dots) and fits to equation 5.22 for the relative front position vs. time. (B): Semi-logarithmic version of (A).

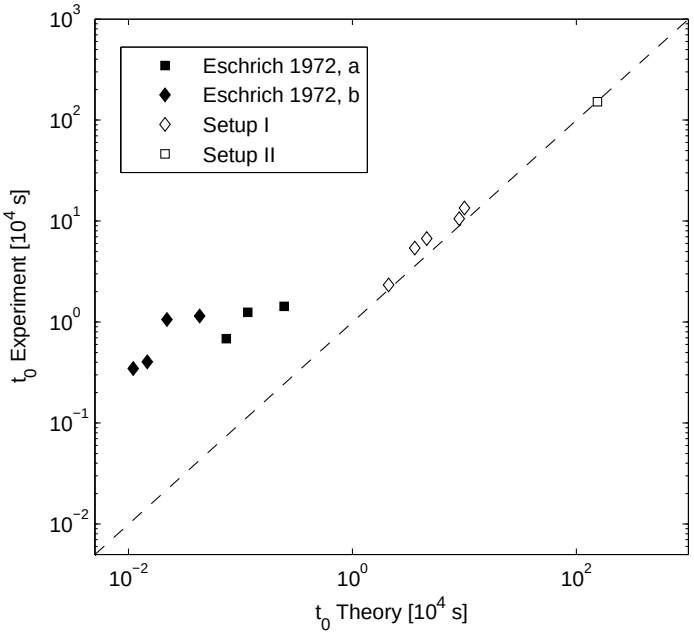

FIGURE 12. Our experimentally obtained values of t_0 plotted together with the results found by Eschrich *et al.* (Eschrich *et al.* 1972). Data points marked with an a represents results from closed tube experiments and points marked with a b represents results from semi-closed experiments take from the original paper, figures 8 and 9.

6. Comparison between theory and experiment

In section 3, we have presented experiments demonstrating the movement of a sugar solution inside a membrane tube surrounded by a reservoir of water. We now wish to consider whether the theory is in agreement with the experimental results.

6.1. *Setup I*

The plot in figure 11 shows the relative front position, $\frac{L-x_f}{L-l}$, plotted against time for five different experiments conducted with setup I. The numbers $1-5$ indicates the sugar concentrations used, cf. table 1. One clearly sees, that the relative front position approaches zero faster for high concentrations than for low. Typical values of M and $\bar{D}$

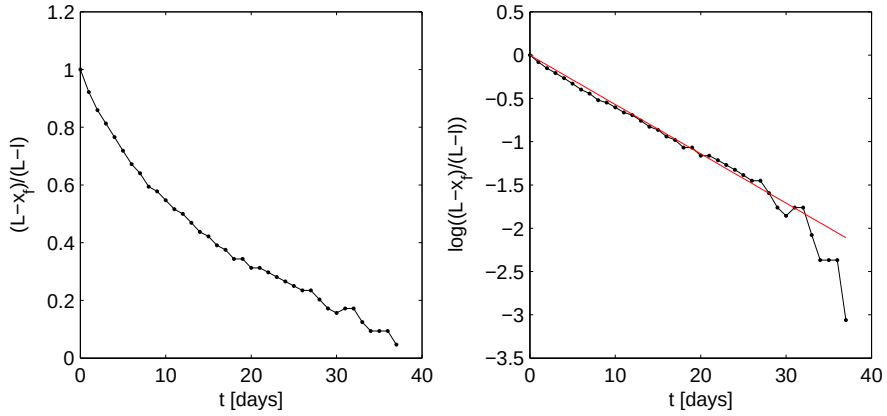

FIGURE 13. Results from setup II showing the relative front position as a function of time.

are $M \sim 10^{-8}$ and $\bar{D} \sim 10^{-5}$, so it is reasonable to assume that we are in the domain where the analytical solution for $M = \bar{D} = 0$ is valid. To test the result from equation 5.19 against the experimental data, the plot in figure 11 shows the logarithm of the relative front position plotted against time. For long stretches of time the curves are seen to approximately follow straight lines in good, qualitative agreement with theory. The red dashed lines are fits to equation (5.19), and we interpret the slopes as $-\frac{1}{t_0}$, the different values plotted in figure 12 against the theoretical values. The theoretically and experimentally obtained values of t_0 are in good quantitative agreement, within 10-30%. Generally, theory predicts somewhat smaller values of t_0 than observed, implying that the observed motion of the sugar front is a little slower than expected from the pressure-flow hypothesis. Nevertheless, as can be seen in figure 12 these results are a considerable improvement to the previous results obtained by Eschrich *et al.* as we find much better agreement between experiment and theory.

6.2. *Setup II*

The plot in figure 13 shows the relative front position, $\frac{L-x_f}{L-l}$, plotted against time for the experiment conducted with setup I. On the semi-logarithmic plot, the curves are seen to follow straight lines in good, qualitative agreement with the simple theory for $M = \bar{D} = 0$. As can be seen in figure 12, we also found very good quantitative agreement between the experiment and theory for setup II.

To test how well the motion of the sugar front observed in the experiments with setup II was reproduced by our model, we solved the equations of motion numerically starting with the initial conditions from figure 5. For $M = \bar{D} = 0$, The results are shown as (red) curves in figure 14 (B). While the front positions are reproduced relatively well, the shape of the front is not, so diffusion must play a role. This can be seen in figure 14 (C) which shows the result of a simulation with $M = 10^{-9}$, $D = 6.9 \times 10^{-11}\mathrm{m}^2\mathrm{s}^{-1}$. Clearly, the model which includes diffusion reproduces the experimental data significantly better.

To study the shape of the front in greater detail, consider the plots on the right in figure 14. Here the gradient of the concentration curves on the left in figure 14 are shown. In (A) we clearly see a peak moving from left to right while it gradually broadens and flattens. In (B) we also see the peak advancing, but the flattening and broadening is much less pronounced. In (C) we see that the model which includes diffusion reproduces the gradual broadening and flattening of the front very well.

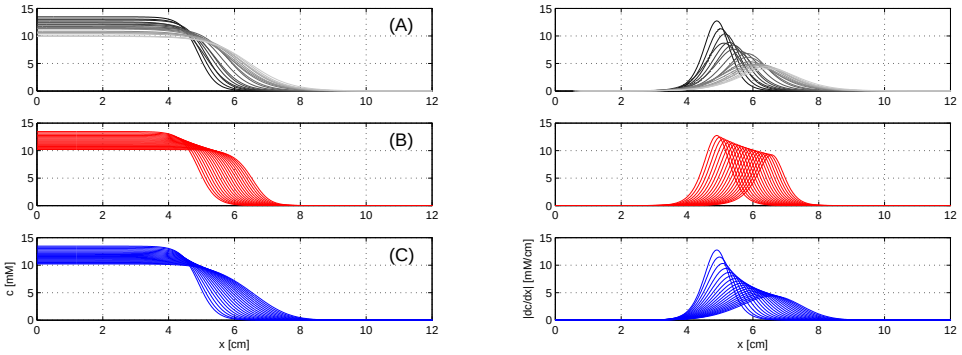

FIGURE 14. Results from setup II showing the experimental data (top row) and the numerical model for $M = D = 0$ (middle row) and for $M = 10^{-9}$, $D = 6.9 \times 10^{-11}\mathrm{m}^2\mathrm{s}^{-1}$ (bottom row).

7. Summary

In this paper we have studied osmotically driven, transient pipe flows. The flows are generated by concentration differences of sugars in closed tubes, fully or partly enclosed by semi-permeable membranes surrounded by pure water. The flows are initiated by a large concentration in one end of the tube and we study the approach to equilibrium, where the sugar is distributed evenly within the tube. Experimentally, we have used two configurations: the first is an updated version of the setup of Eschrich *et al.* where the flow takes place in a dialysis-tube and the sugar is followed by introducing a dye. The advantage is the relatively rapid motion, due to the large surface area. The disadvantage is that the sugar concentration cannot be inferred accurately by this method and for this reason we have introduced our second setup, where the sugar concentration can be followed directly by refraction measurements. On the theoretical side, we first re-derive the governing flow equations and introduce the dimensionless Münch number M. We then show that analytical solutions can be obtained in the two important limits of very large and very small M. In the general case we show how numerical methods based on Green's functions are very effective. Finally, we compare theory and experiment with very good agreement. In particular the results or the velocity of the front (as proposed by Eschrich et al.) can be verified rather accurately.

It is a pleasure to thank Francois Charru, Marie-Alice Goudeau-Boudeville, Hervé Cochard, Pierre Cruiziat, Alexander Schulz, N. Michelle Hollbrook and Vakhtang Putkaradze for many useful discussions. Much appreciated technical assistance was provided by Erik Hansen.

Appendix A. Setup and Methods

A.1. *Materials*

A.1.1. *Chemicals*

The sugar used was a dextran (Sigma-Aldrigde, type D4624) with an average molecular weight of 17.5 kDa. The dye used was a red fruit dye (Flachsmann Scandinavia, Rød Frugtfarve, type 123000) consisting of an aquous mixture of the food additives E-124 and E-131 with molecular weights of 539 Da and 1159 Da respectively (PubChem-Database 2007). Even though the molecular weights are below the MWCO of the membrane, the red dye were not observed to leak through the membrane. This however, was observed

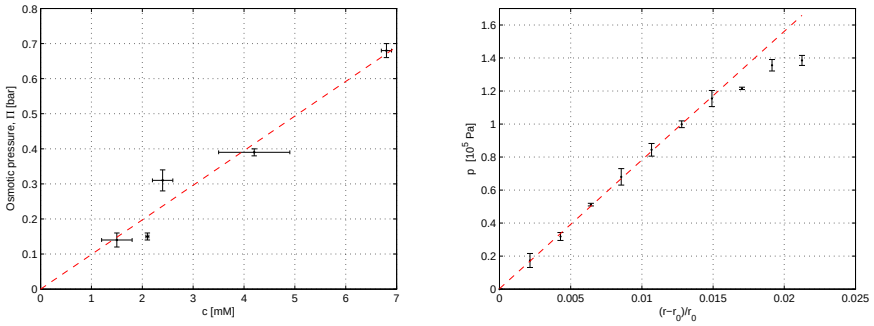

FIGURE 15. Left: van't Hoff relation for $^{17.5\mathrm{kDa}}$Dextran. Right: Elastic properties of the membrane tube

when using another type of dye, Methylene blue, which has a mulecular weight of 320 Da.

A.1.2. *Membrane*

The membrane used in setup I was a semipermeable dialysis membrane tube (Spectra/Por Biotech cellulose ester dialysis membrane) with a radius of 5 mm, thickness 60 μm and a MWCO of 3.5 kDa. The membrane used in setup II had identical specifications except that it had a radius of 3 cm allowing it to cover the interface between the prism and the water reservoir after beeing cut in half.

A.2. *Elastic and osmotic properties of the materials used*

A.2.1. *Elastic properties of the membrane tube*

Figure 15 (right) shows the relation between internal pressure and radius for the membrane tube. For pressures less than 1.2 bar, a linear relation between the relative radial increase and internal pressure was found. Linear elasticity theory (Love 1944) predicts that for a thin-walled cylindrical tube

$$r = r_0 + \frac{r_0^2 p}{dE}, \tag{A 1}$$

where r_0 is the equilibrium radius and d the thickness of the tube, p is pressure and E is Young's modulus of the membrane tube. From this, E, was found to be

$$E = 0.66 \pm 0.01 \text{ GPa} \tag{A 2}$$

A.2.2. *Osmotic strength of Dextran*

Figure 15 (left) shows the relation between dextran concentration and osmotic pressure found from the experiments shown in figure 4. A linear fit gives

$$\Pi = (0.1 \pm 0.01 \text{ bar mM}^{-1})c \tag{A 3}$$

where Π has units of bar, and c is measured in mM. This is in good agreement with values given by (Jonsson 1986)

Appendix B. Tracking the sugar front position

B.1. *Setup I*

After running an experiment with setup I, the raw data we had acquired consisted of a series of pictures as shown in figure 4.

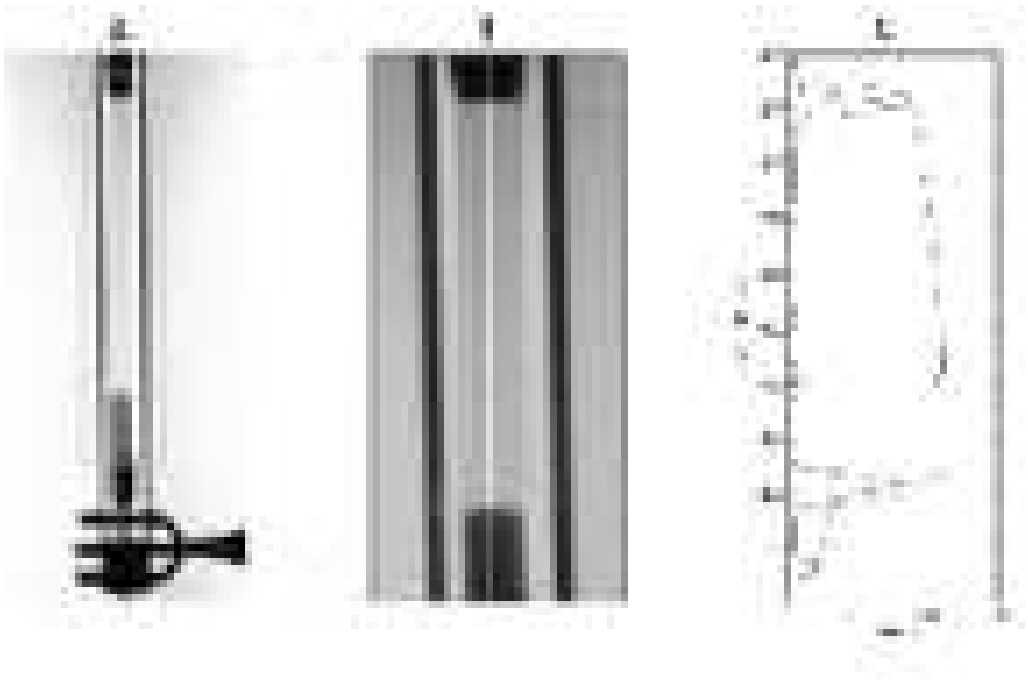

FIGURE 16. Data processesing in setup I.
(A): Raw RGB data image showing the sugar solution mixed with red dye inside the membrane tube.
(B): The image from (A) has been cropped and filtered.
(C): The solid black curve is the intensity of color in (B) taken along the white vertical line. The red curve is the absolute value of the gradient of the intensity. The front position is taken to be where this curve has its maximum value (at approximately 200 pixels). The black dot in (B) is the position of the front found in this manner. The peak in the intensity gradient near 920 pixels is due to the membrane fitting, and was ignored.

To track the position of the sugar-dye front, the images was treated as shown in figure 16. First, the image was imported into MATLAB as (A), and then cropped to shown only the membrane tube, (B). Simultaneously, it was filtered to give the highest contrast for obtaining a well-defined front position. To find the front position, a vertical line running along the center of the membrane tube was picked out, shown as a white line in (B). Along this line, the color intensity was found, shown as the black curve in (C). Finally, the gradient of the color intensity was found – shown in (C) as the red curve – and the front position was defined to be the the position of the maximum in intensity gradient.

To justify the use of red dye as the tracking medium, we took closeup images of the sugar front as shown in figure 17. It is clearly seen, that the dye moves with the point at which the concentration gradient is largest. Thus, we conclude that the dye travels along with the sugar.

B.2. *Setup II*

A camera recorded images of the screen at regular intervals, as shown in figure 6. The deflection at the bottom of the image corresponds to a high sugar concentration inside the lower part of the prism, and the vertical deflection is due to a strong gradient in index of refraction near the sugar front.

As the beam passes through the prism, it gets deflected due to variations in index of refraction of the fluid inside the prism relative to the surrounding air. To determine the

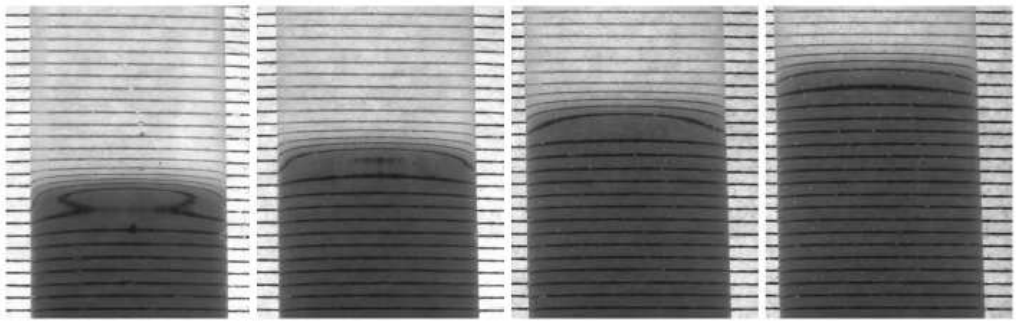

FIGURE 17. Closeup images of the sugar front as it moves. It is clearly seen, that the dye moves with the point at which the concentration gradient is largest.

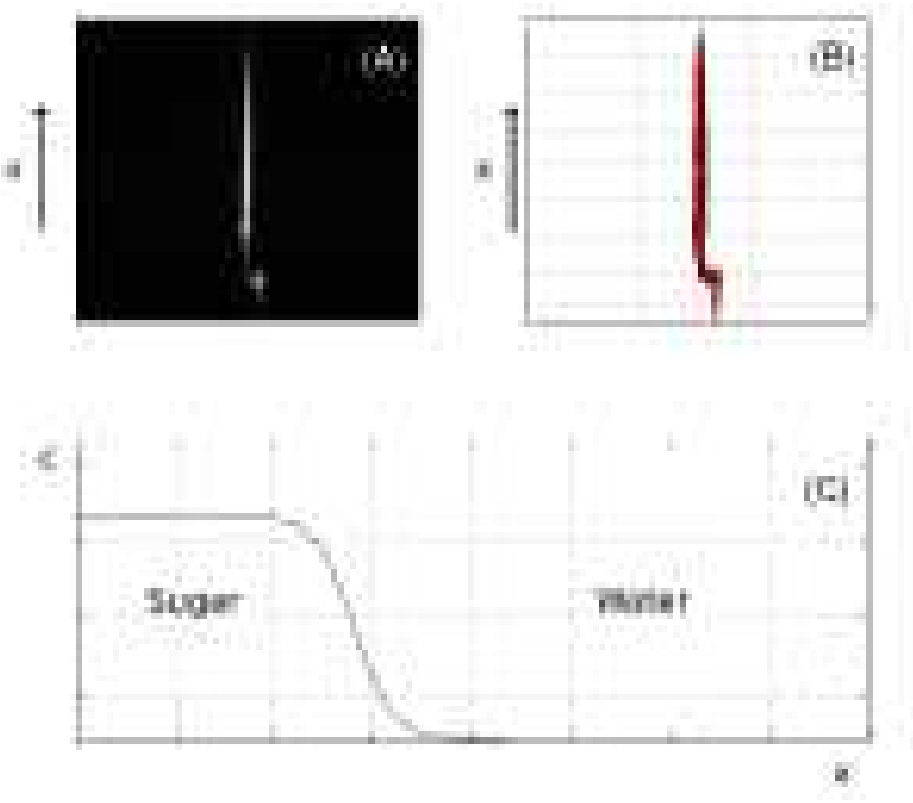

FIGURE 18. Data processing in Setup II. (A): Raw data image. (B): Filtered data image. (C): Index of refraction inside the prism giving the red curve in (B) cf. equation B 5 and B 10

horizontal deflection of a light beam passing through the prism, we consider the situation sketched in figure 19. The deflection Δ_1 along the y axis is given by

$$\Delta_1 = G \tan \Theta_1 \tag{B 1}$$

where G is the orthogonal distance from the prism to the screen, and Θ_1 is the deflection

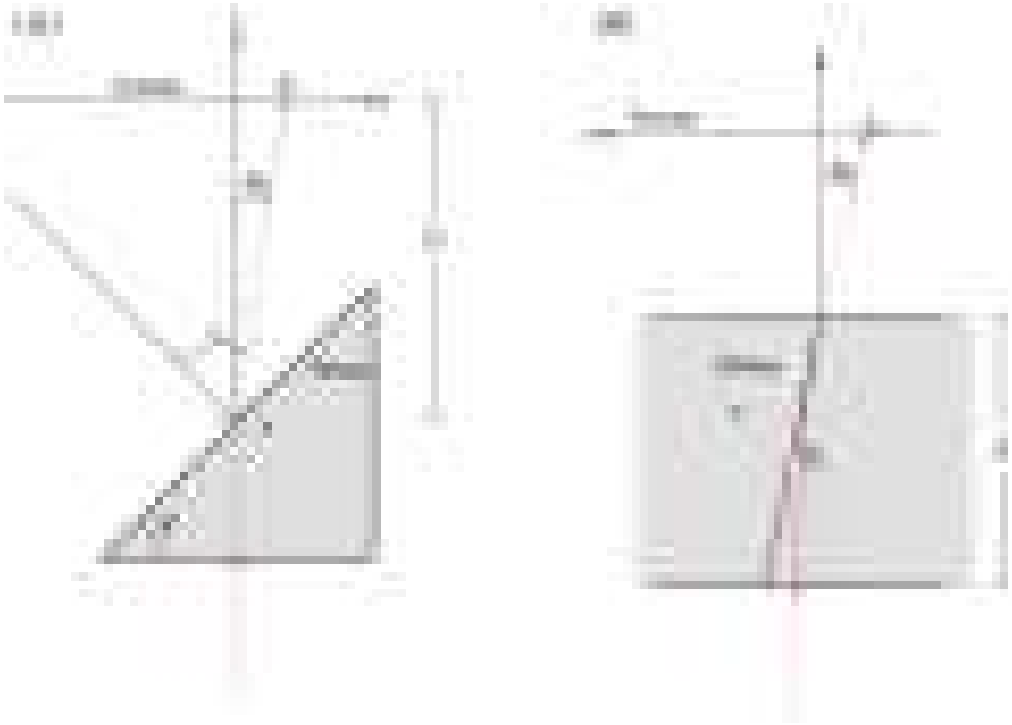

FIGURE 19. Deflection of the laser beam as i passes through the prism.
.

angle as shown in the figure. To find Θ_1 we notice that

$$r_1 - \Theta_1 = \Psi, \tag{B 2}$$

where Ψ is the prism angle. The deflection angle, r_1, is given by the Snell-Descartes law (Hecht 2002)

$$n \sin = \Psi \sin r_1, \tag{B 3}$$

where n is the index of refraction of the fluid inside the prism. In the experiments, Θ_1 is typically small so

$$n \sin \Psi = \sin r_1 = \sin(\Psi + \Theta_1) \simeq \sin \Psi + \Theta_1 \cos \Psi. \tag{B 4}$$

so the horizontal deflection

$$\Delta_1 \simeq G\Theta_1 = G\,(n-1) \tan \Psi. \tag{B 5}$$

To determine the vertical deflection consider the situation sketched in figure 19, (B). According to Fermat's principle, light travels along the path that can be traversed in the least possible time. Consequently, as the light passes through the prism, it travels in a circular arc with a radius of curvature, $\mathcal{R}$, given by

$$\frac{1}{\mathcal{R}} = \mathbf{N} \cdot \frac{\nabla n}{n}, \tag{B 6}$$

where $\mathbf{N}$ is the normal to the trajectory of the light beam Landau & Lifshitz (1984). The vertical deflection is given by

$$\Delta_2 = G \tan \Theta_2 \tag{B 7}$$

where the angle Θ_2 is given by

$$\sin\Theta_2 = n\sin r_2 \tag{B 8}$$

Since r_2 is small, it is clear from the figure that $\sin r_2 \simeq \frac{g}{\mathcal{R}}$, so from equation (B 6)

$$\sin r_2 \simeq \frac{g}{\mathcal{R}} = \frac{g}{n}\frac{\partial n}{\partial x}. \tag{B 9}$$

In the limit where r_2 and Θ_2 are small we get for the vertical deflection

$$\Delta_2 = Gg\frac{\partial n}{\partial x}, \tag{B 10}$$

where we have assumed that ∇n is constant as the beam traverses the prism. Having obtained Δ_1 and Δ_2 we now have to deduce $n(x)$ from the projected image. We will do this by assuming that $n(x)$ has a generic, sigmoid shape

$$n(x) = n_0 + n_1\left(1 - \frac{1}{1+\exp\left(-\frac{x-l}{\epsilon}\right)}\right) \tag{B 11}$$

where the constants n_0 and n_1 controls the magnitude of n and l and ϵ controls the position and steepness of the front. A plot of this function can be seen in figure (18, C)

The procedure for obtaining $n(x)$ was as follows. First, the raw data image was loaded into MATLAB as shown in figure 18, (A). Then, the image was filtered to show only regions of high light intensity, shown as the black dots in (B). Then, a guess of the the form B 11 was made, and the deflections Δ_1 and Δ_2 was calculated from equations B 5 and B 10, shown as the red curve in (B). Finally, an optimization of the parameters was made using MATLAB's `fminsearch` engine, thereby giving the $n(x)$ of the form B 11 best able to reproduce the image seen in (A). Generally, the assumption that n was of the form B 11 gave very good fits, as can be seen in figure 18, (B).

Appendix C. Generalization of the equations of motion to non-cylindrical geometries

When deriving equations 4.19-4.20 we have assumed that our system consisted of a cylindrical tube with semipermeable walls. The assumption of a cylindrical tube, however, have only been used in equation (4.12) where we assumed that the cross-section area to perimeter ratio was

$$\frac{A}{S} = \frac{r}{2} \tag{C 1}$$

and in equation (4.13) where we assumed the axial resistance in Stokes flow to be inversely proportional to the cross-section area

$$\frac{2\pi}{A} = \frac{8}{r^2} \tag{C 2}$$

These two factors are of purely geometrical nature and appear in M, $\bar{D}$ and t_0 as

$$M \propto \frac{2}{r}\cdot\frac{8}{r^2} = \frac{16}{r^3}, \tag{C 3}$$

$$\bar{D} \propto \frac{r}{2} \tag{C 4}$$

and

$$t_0 \propto \frac{r}{2}. \tag{C 5}$$

Therefore, as long as the assumption of a 1D flow velocity and concentration holds inside the tube the equations of motion can be extended to include other geometries, e.g. triangular tubes as used in setup II, by replacing the geometric factors in M, $\bar{D}$ and t_0 as discussed above.

Finding the cross-section area to perimeter ratio is trivial, and the expression for the axial resistance in Stokes flow generally has the form

$$u = \frac{1}{\eta}\frac{A}{\alpha}\frac{\partial p}{\partial x} \tag{C 6}$$

where $\frac{A}{\alpha}$ is a purely geometric factor, which for a cylindrical tube is $\frac{\pi r^2}{8\pi}$. For various pipe cross-sections Mortensen *et al.* (Mortensen *et al.* 2005) has found α as a function of the dimensionless compactness

$$C = \frac{S^2}{A}. \tag{C 7}$$

C.1. *Setup II*

To extend the equations of motion to setup II, consider the following. For a isosceles right triangle with two sides of length s and one of length $\sqrt{2}s$, we get that

$$C = \frac{2(2s+\sqrt{2}s)^2}{s^2} = 12 + 8\sqrt{2} \tag{C 8}$$

Mortensen et. al. showed that for pipes with triangular cross-sections

$$\alpha = \frac{25}{17}C + \frac{40\sqrt{3}}{17} \tag{C 9}$$

so in our case

$$\alpha = \frac{300}{17} + \frac{200\sqrt{2}}{17} + \frac{40\sqrt{3}}{17} \simeq 38.36. \tag{C 10}$$

Also,

$$\frac{A}{S} = \frac{s}{4+2\sqrt{2}}. \tag{C 11}$$

Plugging into the expressions for M, $\bar{D}$ and t_0 we get

$$M^{II} = \frac{38.36(8+4\sqrt{2})\eta L^2 L_p}{(2+\sqrt{2})s^3} = 153.44\frac{\eta L^2 L_p}{s^3}, \tag{C 12}$$

$$\bar{D}^{II} = \frac{(2+\sqrt{2})Ds}{(4+2\sqrt{2})2RTc_0L^2L_p} = \frac{Ds}{2RTc_0L^2L_p} \tag{C 13}$$

and

$$t_0^{II} = \frac{(2+\sqrt{2})s}{(4+2\sqrt{2})L_pRTc_0} = \frac{s}{2L_pRTc_0}. \tag{C 14}$$

The extra factors of $2+\sqrt{2}$ comes from the fact that the membrane only covers one wall of length a, thereby scaling L_p down to $\frac{L_p}{2+\sqrt{2}}$.

Appendix D. Numerical code

```
%%%% 25 Feb 2008 %%%%
%%%% Numerical code for solving the equations of motion %%%%
%%%% for osmotically driven flows in a closed tube %%%%
```

```
%%%% Download at \protect\vrule width0pt\protect\href{http://www.fysik.dtu.dk\string~tbohr/munchsol

function numsolver

%%%% Choose M and D %%%%
D = 1e-8;
M = 1e-8;
a=sqrt(M) ;

%%%% Initialize x and t %%%%
Nx = 500; %
x = linspace(0,1,Nx) ;
Nt = 100;
tspan = linspace(0,40,Nt ) ;

%%%% Initial condition %%%%
epsilon=2e-2;
x0=0.2;
c0=1-1./(1+exp(-(x-x0)/epsilon ));
cbar=trapz (x,c0) ;
for i=2:Nx
    f0(i) = trapz(x(1:i),c0(1:i).cbar);
end

%%%% Run solver %%%%
[t,f] = ode23t (@fderiv,tspan,f0,[],D,a,cbar,x,Nx) ;

%%%% Plot results %%%%
%% Calculate c %%
for i=1:Nt
    c(i,:)=gradient(f(i,:),x)+cbar;
end
%% Plot c %%
figure(1)
surf(c)

%%%% Function fderiv for use in ode23t %%%%
function df = fderiv(t,f,D,a,cbar,x,Nx);
    P = zeros(Nx,1);
    f(1) = 0;
    f(Nx) = 0;
    temp = f';
    f = temp;
    %% Calculate P %%
    for i=2:Nx-2
        P(i) = f(i).(a/sinh(a)).(trapz(x(1:i),...
        sinh(a.(1.x(i)))..f(1:i).....
        sinh(a..x(1:i)))+trapz(x(i+1:end),...
        sinh(a..(1.x(i+1:end)))..f(i+1:end).....
        sinh(a.x(i))));
```

```
end
%% Impose boundary conditions on P %%
P(1) = 0;
P(Nx) = 0;
P(Nx-1) = P(Nx-2)/2;
P=P';
laplacef = 4.del2(f,x);
laplacef(1) = 0;
laplacef(Nx) = 0;
%% Update f %%
df=D*laplacef-P*.(cbar+gradient(f,x));
%% Impose boundary conditions on f %%
df(1) = 0;
df(Nx) = 0;
```

Appendix E. Front propagation in an elastic tube

In this section we shall investigate the effect of expansion of the tube. First we simply assume that water can enter the tube and make it expand without an important increase of pressure. The total volume of the tube is $V = \pi r^2 L$ and the volume of the part with sugar of concentration c_0 is $V = \pi r^2 x$. In the simplest case, we assume that the flow inward only up in he sugar interval $[0, x]$. The rest of the tube just expands without any restoring force ($E = 0$)

$$\frac{dV}{dt} = 2\pi L r \frac{dr}{dt} = \pi r^2 \frac{dx}{dt} + 2\pi r x \frac{dr}{dt} \tag{E 1}$$

Thus

$$(L - x)r^2 = (L - x_0)r_0^2 \tag{E 2}$$

The inflow is

$$I = \frac{dV}{dt} = 2\pi r \int_0^x L_W RTc(x')dx' = 2\pi r L_w RTcx \tag{E 3}$$

But c changes so that $cxr^2 = c_0 x_0 r_0^2$ and thus

$$\frac{dV}{dt} = 2\pi L r \frac{dr}{dt} = \frac{2\pi L_w RTc_0 x_0 r_0^2}{r} \tag{E 4}$$

so

$$\frac{dr}{dt} = \frac{L_w RTc_0 x_0 r_0^2}{Lr^2} \tag{E 5}$$

Note that c_0 os not the average over the whole tube. This would be $\bar{c_0} = \frac{x_0}{L} c_0$. We have earlier introduced the time scale

$$\tau = \frac{r_0}{2L_w RTc_0} \tag{E 6}$$

Using instead

$$\bar{\tau} = \frac{r_0}{2L_w RT\bar{c_0}} \tag{E 7}$$

letting $t = s\bar{\tau}$ and $r = yr_0$ we get

$$y'(s) = \frac{1}{2y^2} \tag{E 8}$$

with solution

$$y(s) = \left(\frac{3s}{2} + 1\right)^{1/3} \tag{E 9}$$

Now x can be found from (E 2):

$$(L - x)y^2 = (L - x_0) \tag{E 10}$$

so

$$x = L - (L - x_0)\left(\frac{3s}{2} + 1\right)^{-2/3} = L - (L - x_0)\left(\frac{3t}{2\tau} + 1\right)^{-2/3} \tag{E 11}$$

Now the front velocity is

$$v(t) = x'(t) = \frac{L - x_0}{\tau}\left(\frac{3t}{2\tau} + 1\right)^{-t/3} \tag{E 12}$$

and initially it takes the value

$$v_0 = x'(0) = \frac{L - x_0}{\tau} \tag{E 13}$$

We now assume that the influx of water creates an increased pressure, and that, consequently water can flow out of the sugarless region. We assume that the elastic properties are governed by

$$p(r) = d_0 E \frac{r - r_0}{r^2} \tag{E 14}$$

where d_0 is the initial width of the membrane, E is Young's modulus and we have assumed incompressibility (i.e. Poisson's ratio $\nu = 1/2$) and, so $dr = d_0 r_0$. Now the equation for the current is

$$I = \frac{dV}{dt} = 2\pi r L_w \int_0^L (RTc(x') - p(x'))\, dx' = 2\pi r L_w (RTc\, x - pL) \tag{E 15}$$

where we have assumed (as in our experiments) that the pressure is constant along the tube. Thus

$$\frac{dV}{dt} = 2\pi r L_W \left(RTc\, x - d_0 E \frac{L(r - r_0)}{r^2}\right) \tag{E 16}$$

Again, $cxr^2 = c_0 x_0 r_0^2$ so

$$\frac{dV}{dt} = 2\pi L r \frac{dr}{dt} = 2\pi r L_w \left(\frac{RTc_0 x_0 r_0^2}{r^2} - d_0 E \frac{L(r - r_0)}{r^2}\right) \tag{E 17}$$

so

$$\frac{dr}{dt} = \frac{L_w RT\bar{c_0} r_0^2}{r^2} - \frac{L_w d_0 E(r - r_0)}{r^2} \tag{E 18}$$

Using again $r = r_0 y$ and $t = \bar{\tau} s$ we get the dimensionless equation

$$\frac{dy}{ds} = \frac{1}{2}\left(\frac{1 - B\,(y - 1)}{y^2}\right) \tag{E 19}$$

where

$$B = \frac{2\bar{\tau} d_0 E L_w}{r_0^2} = \frac{d_0}{r_0}\frac{E}{RT\bar{c_0}} \tag{E 20}$$

In this case we see that the radius saturates for long times to the value:

$$r_f = r_0 y_f = r_0 \frac{1 + B}{B} \tag{E 21}$$

and B can be expressed as

$$B = \frac{1}{y_f - 1} \tag{E 22}$$

This equation can be solved for $s(y)$ by inverting:

$$\frac{ds}{dy} = 2\frac{y^2}{1 + B - By} \tag{E 23}$$

which can be integrated (with the initial condition $s(1) = 0$) to

$$s(y) = \frac{1}{B^3}\left(-(B(y-1)(2 + B(3 + y)) + 2(1 + B)^2 \log(1 + B - By)\right) \tag{E 24}$$

valid as long as $y < y_f$. For small B this is is approximately:

$$s(y) = 1/3(-1 + y^3) + 1/12(1 - 4y^3 + 3y^4)B + o(B^2) \tag{E 25}$$

and thus agrees with the result of last section, i. e. the result for $E \to 0$. For larger B the part of the integral close to

To find the front velocity $v_f = \dot{x}$ we look at the volume $V_2 = \pi r^2(L - x)$ above the sugar front. By definition, the sugar concentration is zero there, so the water flux through the membrane is only due to the pressure difference:

$$\frac{dV_2}{dt} = 2\pi r(L - x)\frac{dr}{dt} - \pi r^2\frac{dx}{dt} = -p(L - x)L_w 2\pi r \tag{E 26}$$

so

$$\frac{1}{L - x}\frac{dx}{dt} = -\frac{d\log(L - x)}{dt} = \frac{2}{r}\left(\frac{dr}{dt} + L_w 2d_0 E\frac{(r - r_0)}{r^2}\right) \tag{E 27}$$

or

$$\begin{aligned}\frac{d\log(L - x)}{ds} &= -\frac{2}{y}\left(\frac{dy}{ds} + \tau r_0^{-2} L_w 2d_0 E\frac{(y-1)}{y^2}\right)\\ &= -\frac{2}{y}\left(\frac{dy}{ds} + B\frac{(y-1)}{y^2}\right)\end{aligned} \tag{E 28}$$

from which we can find $x(t)$ from the solution for $r(t)$, although we cannot write it explicitly since the explicit form of $r(t)$ is not known (only the inverse (E 24)). For $B = 0$ we again recover the flappy limit (E=0), where $L - x \sim y^{-2}$.

REFERENCES

Aldis, G. K. 1988 The unstirred layer during osmotic flow into a tubule. *Bull. Math. Bio.* **50** (5), 531–545.

Barenblatt, G. I. 1996 *Scaling, self-similarity, and intermediate asymptotics*. Cambridge.

Eschrich, Walter, Evert, Ray F. & Young, John H. 1972 Solution flow in tubular semipermeable membranes. *Planta(Berl.)* **107**.

Frisch, H. L. 1976 Osmotically driven flow in narrow channels. *Transactions of the Society of Rheology* **20** (1), 23–27.

Gurbatov, S. N., Malakhov, A. N. & Saichev, Alexander I. 1991 *Nonlinear Random Waves and Turbulence in Nondispersive Media: Waves, Rays, Particles*. Manchester Univ Press.

Hecht, Eugene 2002 *Optics*, 4th edn. Cambridge University Press.

Henton, S.M. 2002 Revisiting the münch pressure-flow hypothesis for long-distance transport of carbohydrates: modelling the dynamics of solute transport inside a semipermeable tube. *J Exp Bot* **53** (373), 1411–1419.

Jonsson, G. 1986 Transport phenomena in ultrafiltration: Membrane selectivity and boundary layer phenomena. *J. Pure and Applied Chemistry* **58** (15), 1647–1656.

Knoblauch, Michael & van Bel, Aart J. E. 1998 Sieve tubes in action. *The Plant Cell* **10**.

Landau, L. D. & Lifshitz, E. M. 1980 *Statistical Physics*, 3rd edn. Pergamon Press.

Landau, L. D. & Lifshitz, E. M. 1984 *Electrodynamics of Continuous Media*. Butterworth-Heinemann.

Love, A. E. H. 1944 *A Treatise on the Mathematical Theory of Elasticity*, 4th edn. Dover.

Mortensen, Niels Asger, Okkels, Fridolin & Bruus, Henrik 2005 Reexamination of hagen-poiseuille flow: Shape dependence of the hydraulic resistance in microchannels. *Physical Review E.* **71**.

Münch, Ernst 1930 *Die Stoffbewegung in der Pflanze*. Jena, Verlag von Gustav Fisher.

Niklas, Karl J. 1992 *Plant Biomechanics – An Engineering Approach to Plant Form and Function*. The University of Chicago Press.

Nobel, Park S. 1999 *Physicochemical & Environmental Plant Physiology*. Academic press.

Pedley, T. J. 1980 The interaction between stirring and osmosis. part 1. *J. Fluid Mech.* **101**.

Pedley, T. J. 1981 The interaction between stirring and osmosis. part 2. *J. Fluid Mech.* **107**.

Pedley, T. J. 1983 Calculation of unstirred layer thickness in membrane transport experiments: a survey. *Quarterly Review of Biophysics* **16** (2), 115–150.

Press, W. H. 2001 *Numerical Recipes in Fortran 77, Volume 1*, 2nd edn. Cambridge University Press.

PubChem-Database 2007 *http://pubchem.ncbi.nlm.nih.gov/*. National Library of Medicine.

Schultz, Stanley G. 1980 *Basic principles of membrane transport*. Cambridge University Press.

Taiz, Lincoln & Zeiger, Eduardo 2002 *Plant Physiology*, 3rd edn. Sinauer Associates, Inc.

Thompson, M. V. & Holbrook, N. M. 2003*a* Application of a single-solute non-steady-state phloem model to the study of long-distance assimilate transport. *J Theo Biol* **220** (4), 419–455.

Thompson, M. V. & Holbrook, N. M. 2003*b* Scaling phloem transport: water potential equilibrium and osmoregulatory flow. *Plant, Cell and Environment* **26**.

Weir, G. J. 1981 Analysis of münch theory. *Mathematical Biosciences* **56**.

An interesting and seminal work on various phenomena in fluid mechanics

ALAN N. OTHER[1]†, H.-C. SMITH[1] AND J. Q. PUBLIC[2]

[1]Department of Chemical Engineering, University of America, Somewhere, IN 12345, USA

[2]Department of Aerospace and Mechanical Engineering, University of Camford, Academic Street, Camford, CF3 5QL, UK

(Received ?? and in revised form ??)

Using Stokes flow between eccentric counter-rotating cylinders as a prototype for bounded nearly parallel lubrication flow, we investigate the effect of a slender recirculation region within the flow field on cross-stream heat or mass transport in the important limit of high Péclet number Pe where the 'enhancement' over pure conduction heat transfer without recirculation is most pronounced. The steady enhancement is estimated with a matched asymptotic expansion to resolve the diffusive boundary layers at the separatrices which bound the recirculation region. The enhancement over pure conduction is shown to vary as $\epsilon^{1/2}$ at infinite Pe, where $\epsilon^{1/2}$ is the characteristic width of the recirculation region. The enhancement decays from this asymptote as $Pe^{-1/2}$.

1. Introduction

The use of integral equations to solve 'exterior' problems in linear acoustics, i.e. to solve the Helmholtz equation $(\nabla^2 + k^2)\phi = 0$ outside a surface S given that ϕ satisfies certain boundary conditions on S, is very common. A good description is provided by **?**. Integral equations have also been used to solve the two-dimensional Helmholtz equation that arises in water-wave problems where there is a constant depth variation. The problem of wave oscillations in arbitrarily shaped harbours using such techniques has been examined (see for example **??**).

In a recent paper **?** have shown how radiation and scattering problems for vertical circular cylinders placed on the centreline of a channel of finite water depth can be solved efficiently using the multipole method devised originally by **?**. This method was also used by **?** to prove the existence of trapped modes in the vicinity of such a cylinder at a discrete wavenumber $k < \pi/2d$ where $2d$ is the channel width.

Many water-wave/body interaction problems in which the body is a vertical cylinder with constant cross-section can be simplified by factoring out the depth dependence. Thus if the boundary conditions are homogeneous we can write the velocity potential $\phi(x, y, z, t) = \mathrm{Re}\{\phi(x, y)\cosh k(z + h)\mathrm{e}^{-\mathrm{i}\omega t}\}$, where the (x, y)-plane corresponds to the undisturbed free surface and z is measured vertically upwards with $z = -h$ the bottom of the channel.

Subsequently **?** proved the existence of, and computed the wavenumbers for, the circular cross-section case. It should be noted however that experimental evidence for acoustic resonances in the case of the circular cylinder is given by **?**, pp. 231–232.

† Present address: Fluid Mech Inc., 24 The Street, Lagos, Nigeria.

? provided a theory for determining the trapped-mode frequencies for the thin plate, based on a modification of the Wiener–Hopf technique. Further interesting results can be found in **?** and **?**.

The use of channel Green's functions, developed in § **??**, allows the far-field behaviour to be computed in an extremely simple manner, whilst the integral equation constructed in § **??** enables the trapped modes to be computed in § **??**. Conclusions are drawn in § **??**. Appendix **??** contains the boundary conditions.

2. Green's functions

2.1. *Construction of equations*

We are concerned with problems for which the solution, ϕ, is either symmetric or antisymmetric about the centreline of the waveguide, $y = 0$. The first step is the construction of a symmetric and an antisymmetric Green's function, $G_s(P, Q)$ and $G_a(P, Q)$. Thus we require

$$(\nabla^2 + k^2)G_s = (\nabla^2 + k^2)G_a = 0 \tag{2.1}$$

in the fluid, where $\boldsymbol{\nabla}$ is a gradient operator,

$$\boldsymbol{\nabla} \cdot \boldsymbol{v} = 0, \quad \nabla^2 P = \boldsymbol{\nabla} \cdot (\boldsymbol{v} \times \boldsymbol{w}).$$

In (**??**)

$$G_s, G_a \sim 1/(2\pi) \ln r \quad \text{as} \quad r \equiv |P - Q| \to 0, \tag{2.2}$$

$$\frac{\partial G_s}{\partial y} = \frac{\partial G_a}{\partial y} = 0 \quad \text{on} \quad y = d, \tag{2.3}$$

$$\left.\begin{aligned} \frac{\partial G_s}{\partial y} = 0 \quad \text{on} \quad y = 0, \\ G_a = 0 \quad \text{on} \quad y = 0, \end{aligned}\right\} \tag{2.4}$$

and we require G_s and G_a to behave like outgoing waves as $|x| \to \infty$.

One way of constructing G_s or G_a is to replace (**??**) and (**??**) by

$$(\nabla^2 + k^2)G_s = (\nabla^2 + k^2)G_a \lesssim -\delta(x - \xi)\delta(y - \eta) \tag{2.5}$$

and to assume initially that k has a positive imaginary part.

2.2. *Further developments*

Using results from **?** we see that this has the integral representation

$$-\frac{1}{2\pi} \int_0^\infty \gamma^{-1} [\mathrm{e}^{-k\gamma|y-\eta|} + \mathrm{e}^{-k\gamma(2d-y-\eta)}] \cos k(x - \xi)t \, \mathrm{d}t, \qquad 0 < y, \quad \eta < d, \tag{2.6}$$

where

$$\gamma(t) = \begin{cases} -\mathrm{i}(1 - t^2)^{1/2}, & t \leqslant 1 \\ (t^2 - 1)^{1/2}, & t > 1. \end{cases}$$

In order to satisfy (**??**) we add to this the function

$$-\frac{1}{2\pi} \int_0^\infty B(t) \frac{\cosh k\gamma(d - y)}{\gamma \sinh k\gamma d} \cos k(x - \xi)t \, \mathrm{d}t$$

which satisfies (**??**), (**??**) and obtain

$$B(t) = 2\mathrm{e}^{-k\gamma d} \cosh k\gamma(d - \eta). \tag{2.7}$$